

Asymmetric Heteroleptic Ir(III) Phosphorescent Complexes with Aromatic Selenide and Selenophene Groups: Synthesis and Photophysical, Electrochemical, and Electrophosphorescent Behaviors

Zhao Feng,[†] Dezhi Wang,[‡] Xiaolong Yang,[†] Deyuan Jin,[†] Daokun Zhong,[†] Boao Liu,[†] Guijiang Zhou,^{*,†} Miaofeng Ma,^{*,‡} and Zhaoxin Wu^{*,§}

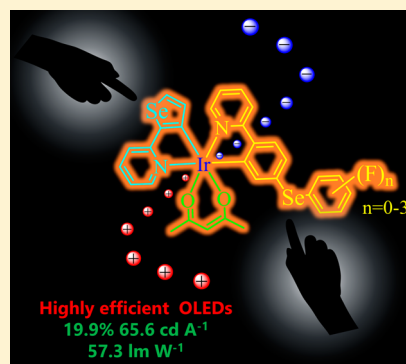
[†]MOE Key Laboratory for Nonequilibrium Synthesis and Modulation of Condensed Matter, Institute of Chemistry for New Energy Materials, Department of Chemistry, School of Science, Xi'an Jiaotong University, Xi'an 710049, People's Republic of China

[‡]Department of Applied Chemistry, College of Chemistry & Pharmacy, Northwest A&F University, Yangling 712100, People's Republic of China

[§]Key Laboratory of Photonics Technology for Information School of Electronic and Information Engineering, Xi'an Jiaotong University, Xi'an 710049, People's Republic of China

Supporting Information

ABSTRACT: With the aim of evaluating the potential of selenium-containing groups in developing electroluminescent (EL) materials, a series of asymmetric heteroleptic Ir(III) phosphorescent complexes (**Ir-Se0F**, **Ir-Se1F**, **Ir-Se2F**, and **Ir-Se3F**) have been synthesized by using 2-selenophenylpyridine and one ppy-type (ppy = 2-phenylpyridine) ligand with a fluorinated selenide group. To the best of our knowledge, these complexes represent unprecedented examples of asymmetric heteroleptic Ir(III) phosphorescent emitters bearing selenium-containing groups. Natural transition orbital (NTO) analysis based on optimized geometries of the first triplet state (T_1) have shown that the phosphorescent emissions of these Ir(III) complexes dominantly show $^3\pi-\pi^*$ features of the 2-selenophenylpyridine ligand with slight metal to ligand charge transfer (MLCT) contribution. In comparison with their symmetric parent complex **Ir-Se** with two 2-selenophenylpyridine ligands, these asymmetric heteroleptic Ir(III) phosphorescent complexes can show much higher phosphorescent quantum yields (Φ_p) of ca. 0.90. Both the hole- and electron-trapping ability of these Ir(III) phosphorescent complexes can be enhanced by selenophene and fluorinated selenide groups to improve their EL efficiencies. The EL abilities of these asymmetric heteroleptic Ir(III) phosphorescent emitters fall in the order **Ir-Se3F** > **Ir-Se2F** > **Ir-Se1F** > **Ir-Se0F**. The highest EL efficiencies have been achieved by **Ir-Se3F** in the solution-processed OLEDs with external quantum efficiency (η_{ext}), current efficiency (η_L), and power efficiency (η_p) of 19.9%, 65.6 cd A^{-1} , and 57.3 lm W^{-1} , respectively. These encouraging EL results clearly indicate the great potential of selenium-containing groups in developing high-performance Ir(III) phosphorescent emitters.



INTRODUCTION

Owing to their distinctive electronic features, elements in group VIA have been widely employed to construct groups to functionalize phosphorescent Ir(III) and Pt(II) complexes with 2-phenylpyridine (ppy)-type ligands, since they can furnish charge carrier injection/transport features to the concerned emissive complexes which can show great potential for making highly efficient organic light-emitting diodes (OLEDs).^{1–8} Typically, these functional groups have been synthesized with oxygen or sulfur atoms embedded into or attached to the aromatic rings.^{5,7,9} Through an attaching strategy, both phenyl ether and phenyl sulfide groups have been introduced to the ppy-type Ir(III) and Pt(II) phosphorescent complexes to enhance their hole injection/hole transport (HI/HT) ability and hence improve electro-

luminescence (EL) efficiencies of the concerned OLEDs.^{7,9} In addition, the phenyl sulfide groups can be converted into phenyl sulfone moieties by proper oxidizing agents to endow the Ir(III) and Pt(II) phosphorescent emitters with enhanced electron injection/electron transport (EI/ET) performance to induce improved EL efficiencies as well.^{1,3,8} Beyond this, aromatic systems with oxygen or sulfur have been employed to synthesize the ppy-type ligands for the Ir(III) and Pt(II) phosphorescent emitters as well.^{3,10–17} To date, several kinds of aromatic units, such as thiophene,^{16,18} benzothio-
 phene,^{13,14,17} benzofuran,^{11,14} dibenzothio-
 phene,^{3,19} dibenzofuran,^{3,20} thiazole,^{21,22} benzothiazole,^{3,23,24} etc., have been

Received: June 13, 2018

introduced to the ppy-type ligands to optimize the EL properties of the Ir(III) and Pt(II) phosphorescent emitters as well. Similarly, as the oxidized counterpart of dibenzothio-phenene, diphenylene sulfone can enhance the EI/ET ability of the ppy-type Ir(III) phosphorescent emitters to bring about attractive EL efficiencies.^{3,25}

In the same group of elements as oxygen and sulfur, selenium can also afford exciting properties with great potential for various applications. In addition to medical activity from the selenides,²⁶ conjugated compounds containing selenophene unit have served as key organic semiconductors in advanced optoelectronic devices, such as organic thin film transistors (OTFTs)^{27,28} and solar cells,^{28,29} exhibiting great potency. Inspired by the success of the phosphorescent emitters with oxygen- and sulfur-containing units in the field of OLEDs, the design and synthesis of phosphorescent analogues bearing selenium-containing groups should definitely represent a feasible strategy to bring about high EL efficiencies in OLEDs. To the best of our knowledge, this aspect has been rarely explored in EL research and only the selenophene unit has been employed to prepare one symmetric *fac*-[Ir(4-phenyl-2-(selenophen-2-yl)quinoline)₃] phosphorescent complex with a phosphorescent quantum yield (Φ_p) of 0.07 to investigate its EL ability.² Considering the critical role played by the Φ_p in enhancing EL performances, improving the Φ_p of selenium-containing Ir(III) phosphorescent emitters should represent an important way to fully explore their potential in the field of OLEDs. Recently, it has been shown that the ppy-type Ir(III) phosphorescent emitters with an asymmetric structure can show obvious advantages over the traditional counterparts adopting a symmetric configuration, since the two different major organic ligands constructing the asymmetric structure can provide great space to optimize the optoelectronic features of the concerned phosphorescent emitters.^{30–32} Taking the advantages of both selenium-containing groups and asymmetric configurations should represent another feasible way to develop new phosphorescent emitters with high EL efficiencies. Bearing all this in mind, we have obtained a series of new asymmetric ppy-type Ir(III) phosphorescent emitters with both selenophene and aryl selenide units to show the potential of selenium-containing groups for constructing functional materials in the EL field. Owing to the unique electronic properties of the selenium-containing groups, all of the investigated ppy-type Ir(III) phosphorescent emitters show impressive EL performances. This research should represent not only a new pathway for developing new phosphorescent emitters with high EL ability but also more comprehensive information about the crucial role played by group VIA elements in the design of high-performance optoelectronic materials.

EXPERIMENTAL SECTION

General Information. Commercially available chemicals were used directly for synthesis with no further purification. All solvents for the reactions were dried and distilled in the proper way. The reactions were monitored with thin-layer chromatography (TLC) materials purchased from Merck & Co., Inc.; silica gel used for flash column chromatography and preparative TLC plates were purchased from Shenghai Qingdao (300–400 mesh). ¹H, ¹⁹F, and ¹³C NMR spectra were measured on a Bruker Avance 400 MHz spectrometer in CDCl₃. Chemical shifts were referenced to the solvent residual peak at δ 7.26 ppm for ¹H and 77.0 ppm for ¹³C NMR spectra, respectively. UV–vis absorption spectra were recorded on a PerkinElmer Lambda 950 spectrophotometer. Emission spectra and lifetimes of these complexes

were measured on an Edinburgh Instruments, Ltd. (FLSP920), fluorescence spectrophotometer. Phosphorescent quantum yields (Φ_p) against *fac*-[Ir(ppy)₃] ($\Phi_p = 0.97$) standard were measured in CH₂Cl₂ solution at 293 K.³³ The differential scanning calorimetry (DSC) and thermal gravimetric analysis (TGA) data were acquired on a NETZSCH DSC 200 PC unit and a NETZSCH STA 409C instrument, respectively. Cyclic voltammetry (CV) was conducted with a Princeton Applied Research Model 273A potentiostat at a 100 mV s⁻¹ scan rate. All of the CV experiments were conducted with a three-electrode compartment cell possessing a Pt-sheet counter electrode, a glassy-carbon working electrode, and an Ag/AgCl reference electrode. The supporting electrolyte was a 0.1 M acetonitrile solution of [*n*Bu₄N]BF₄ with ferrocene as internal reference. The data of elemental analysis were obtained on a Flash EA 1112 elemental analyzer. Fast atom bombardment (FAB) mass spectra were recorded on a Finnigan MAT SSQ710 system. High-resolution mass spectrometry (HRMS) data were obtained on a Waters I-class Vion IMS QToF microspectrometer. FT-IR spectra were acquired on a Bruker Vertex 70 spectrometer.

General Procedure for the Synthesis of Asymmetrical Diaryl Selenones. Under ambient conditions, in a round-bottomed flask charged with 1,2-bis(4-bromophenyl)diselenide (1.0 equiv) were placed the corresponding arylboronic acid (1.5 equiv), CuO nanoparticles (0.03 equiv), and anhydrous DMSO. The reaction mixture was stirred at 100 °C for 24 h. After the reaction mixture was cooled to room temperature, it was poured into a saturated aqueous solution of NaCl and then extracted with petroleum ether three times. The organic phase was dried with anhydrous Na₂SO₄. Then, the solvent was removed under reduced pressure and the residue was redissolved in CHCl₃. To the reaction mixture was added *m*-chloroperbenzoic acid (mCPBA) (5.0 equiv) in small portions at room temperature. After overnight reaction, the reaction mixture was subjected to filtration. The residue was washed with petroleum ether/CH₂Cl₂ (2/1, v/v) twice. The filtrates were combined, and the solvent was removed under reduced pressure. The residue was purified through chromatography on silica gel using CH₂Cl₂ as eluent to gain a pure product.

Br-SeO-0F. Yield: 67.5%. ¹H NMR (400 MHz, CDCl₃, δ): 7.98 (d, *J* = 7.6 Hz, 2H), 7.86 (d, *J* = 8.8 Hz, 2H), 7.75 (d, *J* = 8.4 Hz, 2H), 7.69 (t, *J* = 6.6 Hz, 1H), 7.62 (t, *J* = 7.4 Hz, 2H). ¹³C NMR (100 MHz, CDCl₃, δ): 142.32, 141.38, 134.28, 133.45, 130.37, 129.45, 128.41, 126.86. FAB-MS (*m/z*): 344, 346 [M]⁺. Anal. Calcd for C₁₂H₉BrO₂Se: C, 41.89; H, 2.64. Found: C, 41.78; H, 2.55.

Br-SeO-1F. Yield: 64.3%. ¹H NMR (400 MHz, CDCl₃, δ): 8.00 (tt, *J* = 7.0, 2.0 Hz, 2H), 7.85 (d, *J* = 8.4 Hz, 2H), 7.76 (dt, *J* = 6.8, 1.6 Hz, 2H), 7.31 (t, *J* = 8.6 Hz, 2H). ¹³C NMR (100 MHz, CDCl₃, δ): 166.11 (d, *J* = 256.2 Hz), 141.37, 137.82 (d, *J* = 3.4 Hz), 133.61, 129.76, 129.68 (d, *J* = 3.7 Hz), 128.36, 117.85 (d, *J* = 22.8 Hz). ¹⁹F NMR (376 MHz, CDCl₃, δ): -101.58. FAB-MS (*m/z*): 362, 364 [M]⁺. Anal. Calcd for C₁₂H₈BrFO₂Se: C, 39.81; H, 2.23. Found: C, 39.75; H, 2.11.

Br-SeO-2F. Yield: 57.9%. ¹H NMR (400 MHz, CDCl₃, δ): 7.87 (d, *J* = 8.8 Hz, 2H), 7.79 (d, *J* = 8.8 Hz, 2H), 7.52–7.55 (m, 2H), 7.13 (tt, *J* = 8.4, 2.2 Hz, 1H). ¹³C NMR (100 MHz, CDCl₃, δ): 163.27 (dd, *J* = 257.9, 11.0 Hz), 144.80 (t, *J* = 7.9 Hz), 140.57, 133.79, 130.20, 128.36, 110.79 (dd, *J* = 20.1, 8.5 Hz), 110.16 (t, *J* = 24.8 Hz). ¹⁹F NMR (376 MHz, CDCl₃, δ): -102.53. FAB-MS (*m/z*): 380, 382 [M]⁺. Anal. Calcd for C₁₂H₇BrF₂O₂Se: C, 37.92; H, 1.86. Found: C, 37.82; H, 1.74.

Br-SeO-3F. Yield: 55.1%. ¹H NMR (400 MHz, CDCl₃, δ): 7.85 (d, *J* = 8.8 Hz, 2H), 7.80 (d, *J* = 8.4 Hz, 2H), 7.69 (t, *J* = 5.4 Hz, 2H). ¹³C NMR (100 MHz, CDCl₃, δ): 151.97 (ddd, *J* = 260.1, 10.8, 2.8 Hz), 143.89 (dt, *J* = 262.0, 14.4 Hz), 140.58, 137.48 (dd, *J* = 10.9, 5.4 Hz), 133.90, 130.39, 128.31, 112.46 (dd, *J* = 16.8, 7.6 Hz). ¹⁹F NMR (376 MHz, CDCl₃, δ): -126.49 (d, *J* = 22.6 Hz, 2F), -148.08 (t, *J* = 18.8 Hz, 1F). FAB-MS (*m/z*): 398, 400 [M]⁺. Anal. Calcd for C₁₂H₆BrF₃O₂Se: C, 36.21; H, 1.52. Found: C, 37.05; H, 1.36.

General Procedure for the Synthesis of L-SeO-0F–L-SeO-3F. Under a nitrogen atmosphere, to a solution of Br-SeO-0F/Br-SeO-1F/Br-SeO-2F/Br-SeO-3F (1.1 equiv) and 2-(tributylstannyl)-

pyridine (1.0 equiv) in toluene was added Pd(PPh₃)₄ (0.05 equiv) as catalyst. The reaction mixture was reacted at 110 °C for 20 h. After the mixture was cooled to room temperature, the solvent was removed under vacuum. The residue was purified by column chromatography on silica gel using CH₂Cl₂/ethyl acetate (15/1, v/v) as eluent.

L-SeO-0F. Yield: 85.2%. ¹H NMR (400 MHz, CDCl₃, δ): 8.73 (dd, *J* = 4.8, 0.8 Hz, 1H), 8.24 (dt, *J* = 8.4, 1.8 Hz, 2H), 8.10 (d, *J* = 8.8 Hz, 2H), 8.02 (dt, *J* = 6.8, 1.6 Hz, 2H), 7.82 (td, *J* = 7.6, 2.0 Hz, 1H), 7.77 (d, *J* = 8.0 Hz, 1H), 7.68 (tt, *J* = 7.4, 2.0 Hz, 1H), 7.62 (t, *J* = 7.4 Hz, 2H), 7.33 (ddd, *J* = 7.0, 4.8, 1.4 Hz, 1H). ¹³C NMR (100 MHz, CDCl₃, δ): 154.93, 150.14, 144.97, 142.69, 142.44, 137.17, 134.12, 130.30, 128.61, 127.45, 126.96, 123.56, 121.16. FAB-MS (*m/z*): 343 [M]⁺. Anal. Calcd for C₁₇H₁₃NO₂Se: C, 59.66; H, 3.83; N, 4.09. Found: C, 59.56; H, 3.72; N, 3.92.

L-SeO-1F. Yield: 82.3%. ¹H NMR (400 MHz, CDCl₃, δ): 8.73 (dd, *J* = 3.0, 0.4 Hz, 1H), 8.24 (d, *J* = 8.8 Hz, 2H), 8.08 (dd, *J* = 6.8, 1.6 Hz, 2H), 8.04 (t, *J* = 7.0, 2.0 Hz, 2H), 7.82 (td, *J* = 7.7, 2.0 Hz, 1H), 7.77 (d, *J* = 8.0 Hz, 1H), 7.28–7.35 (m, 3H). ¹³C NMR (100 MHz, CDCl₃, δ): 165.96 (d, *J* = 255.8 Hz), 154.78, 150.13, 145.09, 142.32, 138.11 (d, *J* = 2.8 Hz), 137.15, 129.69 (d, *J* = 9.5 Hz), 128.66, 127.31, 123.58, 121.13, 117.68 (d, *J* = 22.7 Hz). ¹⁹F NMR (376 MHz, CDCl₃, δ): –102.07. FAB-MS (*m/z*): 361 [M]⁺. Anal. Calcd for C₁₇H₁₂FNO₂Se: C, 56.68; H, 3.36; N, 3.89. Found: C, 59.57; H, 3.24; N, 3.79.

L-SeO-2F. Yield: 84.7%. ¹H NMR (400 MHz, CDCl₃, δ): 8.73 (d, *J* = 4.4 Hz, 1H), 8.27 (d, *J* = 8.8 Hz, 2H), 8.09 (d, *J* = 8.4 Hz, 2H), 7.83 (tt, *J* = 7.6, 1.6 Hz, 1H), 7.79 (d, *J* = 8.0 Hz, 1H), 7.56–7.58 (m, 2H), 7.35 (ddd, *J* = 7.2, 4.8, 1.6 Hz, 1H), 7.11 (tt, *J* = 8.4, 2.4 Hz, 1H). ¹³C NMR (100 MHz, CDCl₃, δ): 163.26 (dd, *J* = 257.7, 11.0 Hz), 154.58, 150.18, 145.53, 145.20 (t, *J* = 7.8 Hz), 141.56, 137.20, 128.86, 127.39, 123.70, 121.17, 110.79 (dd, *J* = 20.1, 8.5 Hz), 109.94 (t, *J* = 24.8 Hz). ¹⁹F NMR (376 MHz, CDCl₃, δ): –102.87. FAB-MS (*m/z*): 379 [M]⁺. Anal. Calcd for C₁₇H₁₁F₂NO₂Se: C, 53.98; H, 2.93; N, 3.70. Found: C, 53.87; H, 2.85; N, 3.59.

L-SeO-3F. Yield: 83.6%. ¹H NMR (400 MHz, CDCl₃, δ): 8.74 (d, *J* = 4.4 Hz, 1H), 8.28 (dd, *J* = 6.8, 1.6 Hz, 2H), 8.08 (dd, *J* = 7.2, 1.6 Hz, 2H), 7.83 (td, *J* = 7.6, 1.6 Hz, 1H), 7.79 (d, *J* = 7.6 Hz, 1H), 7.72 (t, *J* = 5.6 Hz, 2H), 7.35 (ddd, *J* = 7.0, 5.0, 1.2 Hz, 1H). ¹³C NMR (150 MHz, CDCl₃, δ): 154.49, 151.81 (ddd, *J* = 259.8, 10.9, 2.4 Hz), 150.20, 145.65, 143.75 (dt, *J* = 261.1, 14.63 Hz), 141.57, 137.89 (dd, *J* = 10.5, 5.3 Hz), 137.20, 128.92, 127.32, 123.74, 121.15, 112.46 (dd, *J* = 18.2, 5.9 Hz). ¹⁹F NMR (376 MHz, CDCl₃, δ): –126.87 (d, *J* = 22.6 Hz, 2F), –148.62 (t, *J* = 18.8 Hz, 1F). FAB-MS (*m/z*): 397 [M]⁺. Anal. Calcd for C₁₇H₁₀F₃NO₂Se: C, 51.53; H, 2.54; N, 3.54. Found: C, 51.43; H, 2.45; N, 3.39.

General Procedure for the Synthesis of L-SeO–L-Se3F.

Under a nitrogen atmosphere, to a mixture of L-SeO-0F/L-SeO-1F/L-SeO-2F/L-SeO-3F (1.0 equiv) and Pd/C (0.01 equiv, 10 wt % Pd content) in ethanol was added hydrazine hydrate (3.0 equiv). The reaction mixture was allowed to react at 60 °C for 6 h. After it was cooled to room temperature, the mixture was filtered and the residue was washed with CH₂Cl₂. Then, the solvent was removed under reduced pressure and the resultant residue was purified by column chromatography on silica gel using CH₂Cl₂/petroleum ether (1/1, v/v) as eluent.

L-Se0F. Yield: 89.7%. ¹H NMR (400 MHz, CDCl₃, δ): 8.68 (dd, *J* = 4.0, 0.8 Hz, 1H), 7.89 (dd, *J* = 6.4, 1.6 Hz, 2H), 7.75 (td, *J* = 7.6, 1.6 Hz, 1H), 7.70 (dd, *J* = 6.8, 1.2 Hz, 1H), 7.55 (dt, *J* = 8.4, 2.0 Hz, 2H), 7.49–7.52 (m, 2H), 7.29 (t, *J* = 3.0 Hz, 3H), 7.23 (ddd, *J* = 7.2, 4.8, 1.2 Hz, 1H). ¹³C NMR (100 MHz, CDCl₃, δ): 156.74, 149.73, 138.38, 136.78, 133.22, 132.97, 132.59, 130.78, 129.39, 127.70, 127.51, 122.23, 120.34. FAB-MS (*m/z*): 311 [M]⁺. Anal. Calcd for C₁₇H₁₃NSe: C, 65.81; H, 4.22; N, 4.51. Found: C, 65.74; H, 4.09; N, 4.36.

L-Se1F. Yield: 85.4%. ¹H NMR (400 MHz, CDCl₃, δ): 8.68 (d, *J* = 4.8 Hz, 1H), 7.88 (dd, *J* = 6.6, 1.8 Hz, 2H), 7.74 (td, *J* = 7.6, 2.0 Hz, 1H), 7.69 (dt, *J* = 8.0, 0.8 Hz, 1H), 7.54–7.50 (m, 2H), 7.48 (dt, *J* = 8.8, 2.0 Hz, 2H), 7.23 (ddd, *J* = 7.2, 4.8, 1.2 Hz, 1H), 7.01 (tt, *J* = 9.0, 2.4 Hz, 2H). ¹³C NMR (100 MHz, CDCl₃, δ): 162.67 (d, *J* = 246.3

Hz), 156.65, 149.72, 138.28, 136.79, 135.91 (d, *J* = 7.9 Hz), 133.08, 132.21, 127.72, 124.87 (d, *J* = 3.4 Hz), 122.25, 120.31, 116.64 (d, *J* = 21.3 Hz). ¹⁹F NMR (376 MHz, CDCl₃, δ): –113.69. FAB-MS (*m/z*): 329 [M]⁺. Anal. Calcd for C₁₇H₁₂FNSe: C, 62.21; H, 3.69; N, 4.27. Found: C, 62.08; H, 3.59; N, 4.17.

L-Se2F. Yield: 88.3%. ¹H NMR (400 MHz, CDCl₃, δ): 8.71 (d, *J* = 4.4 Hz, 1H), 7.98 (dd, *J* = 6.8, 1.6 Hz, 2H), 7.78 (td, *J* = 7.4, 1.6 Hz, 1H), 7.74 (d, *J* = 8.0 Hz, 1H), 7.67 (dt, *J* = 8.4, 1.8 Hz, 2H), 7.25–7.28 (m, 1H), 6.88 (dd, *J* = 7.2, 2.4 Hz, 2H), 6.66 (tt, *J* = 8.8, 2.2 Hz, 1H). ¹³C NMR (100 MHz, CDCl₃, δ): 163.06 (dd, *J* = 250.4, 12.4 Hz), 156.38, 149.82, 139.81, 136.90, 135.48 (t, *J* = 8.7 Hz), 135.18, 129.35, 128.17, 122.57, 120.58, 113.79 (dd, *J* = 19.3, 6.9 Hz), 102.38 (t, *J* = 25.4 Hz). ¹⁹F NMR (376 MHz, CDCl₃, δ): –109.18. FAB-MS (*m/z*): 347 [M]⁺. Anal. Calcd for C₁₇H₁₁F₂NSe: C, 58.97; H, 3.20; N, 4.05. Found: C, 58.89; H, 3.11; N, 3.96.

L-Se3F. Yield: 86.1%. ¹H NMR (400 MHz, CDCl₃, δ): 8.70 (d, *J* = 4.8 Hz, 1H), 7.97 (dd, *J* = 6.6, 1.8 Hz, 2H), 7.78 (td, *J* = 7.6, 1.6 Hz, 1H), 7.73 (d, *J* = 7.6 Hz, 1H), 7.62 (dt, *J* = 8.8, 2.0 Hz, 2H), 7.25–7.28 (m, 1H), 7.03 (t, *J* = 7.0 Hz, 2H). ¹³C NMR (100 MHz, CDCl₃, δ): 156.33, 151.35 (ddd, *J* = 252.4, 10.3, 3.7 Hz), 149.84, 138.98 (dt, *J* = 250.5, 15.3 Hz), 139.76, 136.90, 134.56, 129.93, 128.20, 126.68 (dd, *J* = 12.2, 6.8 Hz), 122.58, 120.55, 115.88 (dd, *J* = 16.2, 6.0 Hz). ¹⁹F NMR (376 MHz, CDCl₃, δ): –133.27 (d, *J* = 22.6 Hz, 2F), –161.51 (t, *J* = 18.8 Hz, 1F). FAB-MS (*m/z*): 365 [M]⁺. Anal. Calcd for C₁₇H₁₀F₃NSe: C, 56.06; H, 2.77; N, 3.85. Found: C, 55.95; H, 2.68; N, 3.79.

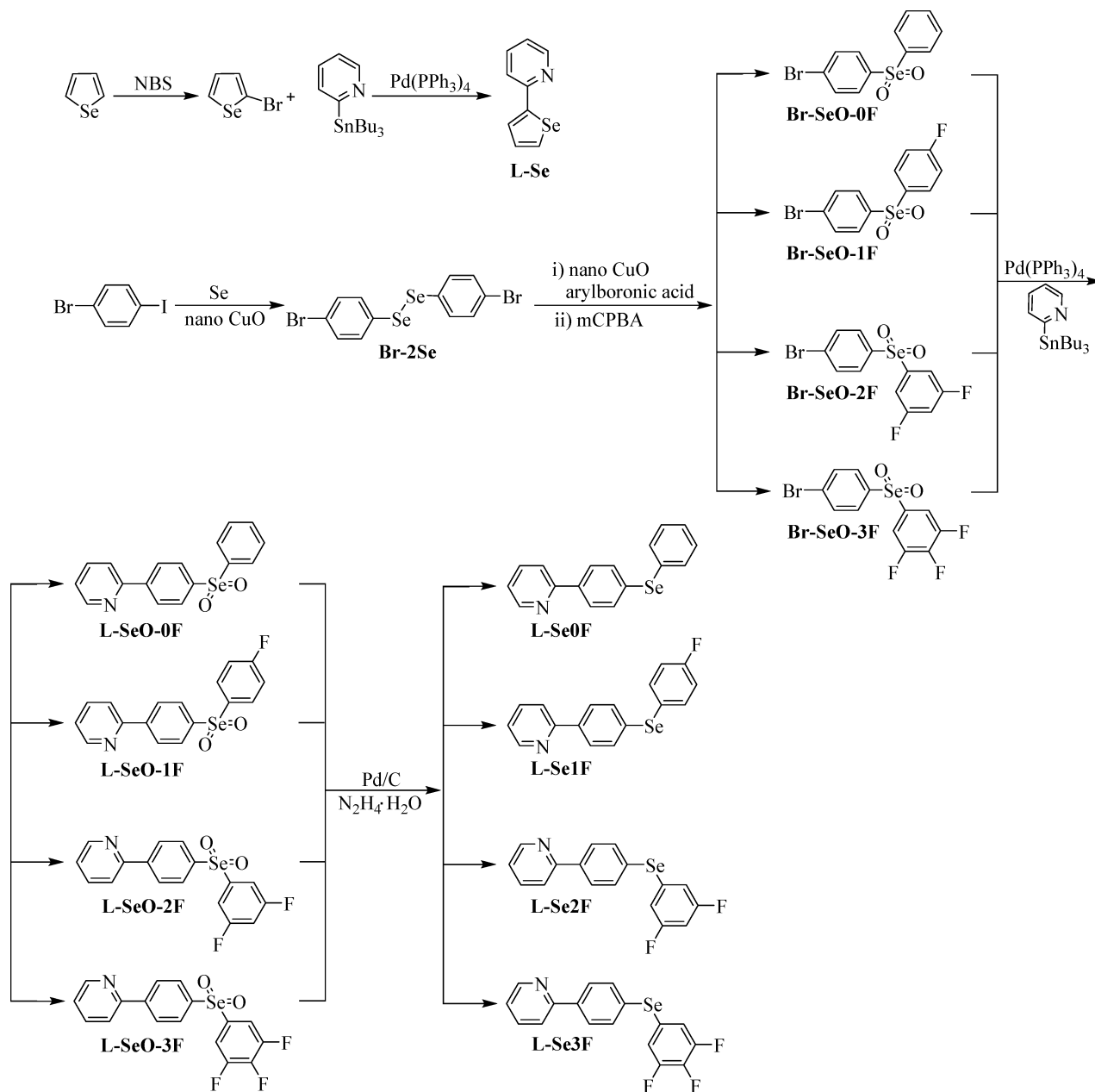
2-(Selenophen-2-yl)pyridine (L-Se). Under a nitrogen atmosphere, to a solution of 2-bromoselenophene (2.00 g, 9.5 mmol) and 2-(tributylstannyl)pyridine (3.50 g, 9.5 mmol) in toluene was added Pd(PPh₃)₄ (0.55 g, 0.47 mmol) as catalyst. The reaction was allowed to proceed at 110 °C for 20 h. After the reaction mixture was cooled to room temperature, the solvent was removed under reduced pressure. The residue was chromatographed with a silica gel column using CH₂Cl₂/petroleum ether (1/3, v/v) as eluent. The product was obtained as a colorless solid (1.65 g, 83.8%). ¹H NMR (400 MHz, CDCl₃, δ): 8.53 (d, *J* = 4.8 Hz, 1H), 8.05 (dd, *J* = 5.6, 0.8 Hz, 1H), 7.74 (dd, *J* = 4.0, 0.8 Hz, 1H), 7.66 (dd, *J* = 4.8, 1.2 Hz, 2H), 7.37 (t, *J* = 4.8 Hz, 1H), 7.14 (dd, *J* = 8.8, 4.8 Hz, 1H). ¹³C NMR (100 MHz, CDCl₃, δ): 154.02, 151.75, 149.64, 136.53, 132.84, 130.72, 126.07, 121.92, 117.79. FAB-MS (*m/z*): 209 [M]⁺. Anal. Calcd for C₉H₇NSe: C, 51.94; H, 3.39; N, 6.73. Found: C, 51.87; H, 3.28; N, 6.65.

General Procedure for the Synthesis of Ir-Se0F–Ir-Se3F.

Under a nitrogen atmosphere, to a mixture of THF and H₂O (3/1, v/v) were added L-Se (1.0 equiv) and IrCl₃·*n*H₂O (0.9 equiv, 60 wt % Ir content). The reaction mixture was stirred at 80 °C for 2 h. After the mixture was cooled to room temperature, L-Se0F/L-Se1F/L-Se2F/L-Se3F (1.0 equiv) was added under a nitrogen flow, and then the resulting mixture was stirred at 110 °C for another 8 h. After it was cooled to room temperature, the reaction mixture was extracted with CH₂Cl₂ three times. The organic phases were combined and dried with anhydrous Na₂SO₄. After most of the solvent was removed, the colored Ir(III) μ -chloro-bridged dimer was precipitated with petroleum ether; the precipitate was obtained through centrifugation and dried under vacuum. Subsequently, thallium(I) acetylacetonate [Tl(acac)] (2.2 equiv) was added to an anhydrous CH₂Cl₂ solution of the colored Ir(III) μ -chloro-bridged dimer (1.0 equiv). The reaction mixture was allowed to react at room temperature overnight. Centrifugation was conducted to remove the inorganic salt, and the solvent was removed under vacuum from the organic phase. The residue was purified with preparative thin-layer chromatography (TLC) made of silica gel using proper eluent. Caution: thallium(I) acetylacetonate (Tl(acac)) is extremely toxic and must be dealt with carefully.

Ir-Se0F. Yield: 26.2%. ¹H NMR (400 MHz, CDCl₃, δ): 8.48 (d, *J* = 5.6 Hz, 1H), 8.18 (d, *J* = 6.0 Hz, 1H), 7.79–7.76 (m, 2H), 7.69 (td, *J* = 7.8, 1.2 Hz, 1H), 7.48 (t, *J* = 7.8 Hz, 1H), 7.36 (d, *J* = 8.0 Hz, 1H), 7.34–7.30 (m, 3H), 7.21–7.16 (m, 3H), 7.11 (t, *J* = 6.0 Hz, 1H), 6.84 (dd, *J* = 8.0, 1.6 Hz, 1H), 6.81 (dd, *J* = 6.6, 1.2 Hz, 1H), 6.28 (d, *J* = 1.6 Hz, 1H), 6.22 (d, *J* = 5.2 Hz, 1H), 5.21 (s, 1H), 1.79 (s, 3H), 1.78 (s, 3H). ¹³C NMR (100 MHz, CDCl₃, δ): 184.63, 184.46,

Scheme 1. Synthetic Scheme for the Organic Ligands



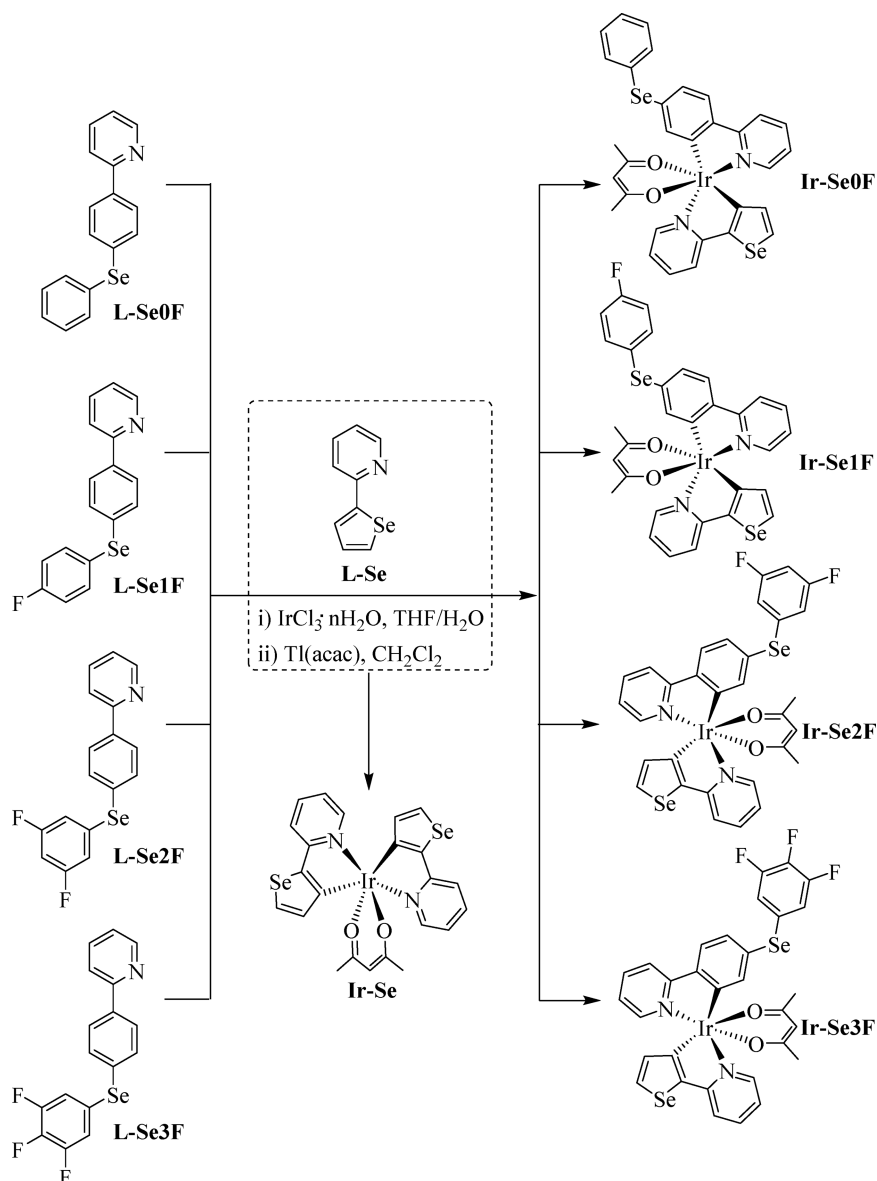
168.41, 166.40, 153.22, 148.32, 147.87, 147.06, 143.61, 137.39, 136.84, 135.97, 135.87, 134.92, 133.50, 133.03, 132.93, 130.64, 129.09, 127.03, 123.90, 123.79, 121.16, 118.32, 118.23, 118.10, 100.43, 28.65, 28.61. HRMS-ESI Calcd for $\text{C}_{31}\text{H}_{25}\text{IrN}_2\text{O}_2\text{Se}_2$ 809.9876, found 807.9848 $[\text{M} + \text{H}]^+$. Anal. Calcd for $\text{C}_{31}\text{H}_{25}\text{IrN}_2\text{O}_2\text{Se}_2$: C, 46.10; H, 3.12; N, 3.47. Found: C, 45.95; H, 3.02; N, 3.39.

Ir-Se1F. Yield: 25.8%. ^1H NMR (400 MHz, CDCl_3 , δ): 8.46 (d, $J = 5.6$ Hz, 1H), 8.13 (d, $J = 5.6$ Hz, 1H), 7.78–7.76 (m, 2H), 7.69 (td, $J = 7.6$ Hz, 1H), 7.52 (td, $J = 8.0, 1.6$ Hz, 1H), 7.35 (d, $J = 8.0$ Hz, 1H), 7.33–7.28 (m, 3H), 7.10 (td, $J = 6.6, 1.2$ Hz, 1H), 6.87 (t, $J = 8.8$ Hz, 2H), 6.83–6.78 (m, 2H), 6.22 (d, $J = 5.2$ Hz, 1H), 6.03 (d, $J = 2.0$ Hz, 1H), 5.20 (s, 1H), 1.79 (s, 3H), 1.78 (s, 3H). ^{13}C NMR (100 MHz, CDCl_3 , δ): 184.66, 184.43, 168.37, 166.37, 162.44 (d, $J = 245.3$ Hz), 153.32, 148.32, 147.84, 147.26, 143.28, 137.30, 136.86, 136.68 (d, $J = 7.9$ Hz), 135.78, 134.99, 134.44, 134.05, 132.96, 124.29 (d, $J = 3.1$ Hz), 123.76, 122.50, 121.10, 118.20, 118.17, 117.98, 116.30 (d, $J = 21.4$ Hz), 100.44, 28.65, 28.60. ^{19}F NMR (376 MHz, CDCl_3 , δ): –114.22. HRMS-ESI: calcd for $\text{C}_{31}\text{H}_{24}\text{FIrN}_2\text{O}_2\text{Se}_2$ 827.9781, found

825.9769 $[\text{M} + \text{H}]^+$. Anal. Calcd for $\text{C}_{31}\text{H}_{24}\text{FIrN}_2\text{O}_2\text{Se}_2$: C, 45.10; H, 2.93; N, 3.39. Found: C, 45.01; H, 2.86; N, 3.28.

Ir-Se2F. Yield: 30.3%. ^1H NMR (400 MHz, CDCl_3 , δ): 8.51 (d, $J = 5.2$ Hz, 1H), 8.20 (d, $J = 5.6$ Hz, 1H), 7.83–7.79 (m, 2H), 7.73 (td, $J = 7.4, 1.6$ Hz, 1H), 7.52 (td, $J = 7.4, 1.2$ Hz, 1H), 7.43 (d, $J = 8.0$ Hz, 1H), 7.38 (d, $J = 8.0$ Hz, 1H), 7.15 (td, $J = 6.4, 1.6$ Hz, 1H), 6.95 (dd, $J = 8.0, 1.6$ Hz, 1H), 6.84 (td, $J = 6.6, 1.2$ Hz, 1H), 6.77 (dd, $J = 7.2, 2.0$ Hz, 2H), 6.60 (tt, $J = 8.8, 2.0$ Hz, 1H), 6.31 (d, $J = 1.6$ Hz, 1H), 6.22 (d, $J = 5.2$ Hz, 1H), 5.23 (s, 1H), 1.81 (s, 3H), 1.80 (s, 3H). ^{13}C NMR (100 MHz, CDCl_3 , δ): 184.73, 184.56, 168.15, 166.51, 162.73 (dd, $J = 249.9, 12.3$ Hz), 153.06, 148.44, 147.88, 147.84, 144.85, 137.51, 137.39, 136.98, 135.91, 135.01 (t, $J = 8.9$ Hz), 134.75, 133.22, 130.23, 125.12, 124.14, 121.58, 118.50, 118.33, 118.09, 114.69 (dd, $J = 19.0, 6.8$ Hz), 102.23 (t, $J = 25.2$ Hz), 100.48, 28.65, 28.59. ^{19}F NMR (376 MHz, CDCl_3 , δ): –109.52. HRMS-ESI: calcd for $\text{C}_{31}\text{H}_{23}\text{F}_2\text{IrN}_2\text{O}_2\text{Se}_2$ 845.9687, found 843.9482 $[\text{M} + \text{H}]^+$. Anal. Calcd for $\text{C}_{31}\text{H}_{23}\text{F}_2\text{IrN}_2\text{O}_2\text{Se}_2$: C, 44.13; H, 2.75; N, 3.32. Found: C, 44.02; H, 2.68; N, 3.18.

Scheme 2. Synthetic Scheme for the Asymmetric ppy-Type Ir(III) Phosphorescent Emitters with both Selenophene and Aryl Selenide Units Together with Their Parent Complex Ir-Se



Ir-Se3F. Yield: 31.1%. ^1H NMR (400 MHz, CDCl_3 , δ): 8.48 (d, J = 5.2 Hz, 1H), 8.17 (d, J = 5.6 Hz, 1H), 7.81–7.79 (m, 2H), 7.72 (td, J = 7.4, 1.6 Hz, 1H), 7.55 (td, J = 7.4, 1.2 Hz, 1H), 7.41 (d, J = 8.0 Hz, 1H), 7.37 (d, J = 8.0 Hz, 1H), 7.14 (td, J = 6.6, 1.2 Hz, 1H), 6.94–6.88 (m, 3H), 6.84 (td, J = 6.6, 1.2 Hz, 1H), 6.21 (d, J = 5.2 Hz, 1H), 6.07 (d, J = 1.6 Hz, 1H), 5.22 (s, 1H), 1.80 (s, 3H), 1.79 (s, 3H). ^{13}C NMR (100 MHz, CDCl_3 , δ): 184.74, 184.52, 168.06, 166.48, 153.11, 150.86 (ddd, J = 251.8, 10.0, 3.5 Hz), 148.39, 147.88, 147.81, 144.35, 139.11 (dt, J = 249.7, 15.1 Hz), 137.36, 136.99, 135.82, 135.59, 134.79, 133.27, 131.59, 125.26 (dd, J = 12.1, 6.6 Hz), 123.98, 123.58, 121.49, 118.41, 118.17, 117.89, 117.71 (dd, J = 16.2, 5.6 Hz), 100.51, 28.64, 28.59. ^{19}F NMR (376 MHz, CDCl_3 , δ): –133.53 (d, J = 22.6 Hz, 2F), –161.27 (t, J = 18.8 Hz, 1F). HRMS-ESI: calcd for $\text{C}_{31}\text{H}_{22}\text{F}_3\text{IrN}_2\text{O}_2\text{Se}_2$, 863.9593, found 861.9590 $[\text{M} + \text{H}]^+$. Anal. Calcd for $\text{C}_{31}\text{H}_{22}\text{F}_3\text{IrN}_2\text{O}_2\text{Se}_2$: C, 43.21; H, 2.57; N, 3.25. Found: C, 43.08; H, 2.48; N, 3.16.

Ir-Se. Yield: 20.3–24.1%. ^1H NMR (400 MHz, CDCl_3 , δ): 8.32 (d, J = 5.6 Hz, 2H), 7.81 (d, J = 5.2 Hz, 2H), 7.58 (td, J = 8.0, 1.2 Hz, 2H), 7.44 (d, J = 8.0 Hz, 2H), 6.92 (td, J = 6.6, 1.2 Hz, 2H), 6.33 (d, J = 5.2 Hz, 2H), 5.22 (s, 1H), 1.81 (s, 6H). ^{13}C NMR (100 MHz, CDCl_3 , δ): 184.51, 167.04, 152.18, 148.16, 137.43, 135.74, 135.31,

132.86, 118.17, 118.00, 100.52, 28.54. HRMS (ESI): calcd for $\text{C}_{23}\text{H}_{19}\text{IrN}_2\text{O}_2\text{Se}_2$, 707.9406, found 705.9380 $[\text{M} + \text{H}]^+$. Anal. Calcd for $\text{C}_{23}\text{H}_{19}\text{IrN}_2\text{O}_2\text{Se}_2$: C, 39.15; H, 2.71; N, 3.97. Found: C, 39.08; H, 2.76; N, 3.88%.

X-ray Crystallography. Single crystals of Ir-Se2F and Ir-Se3F that were suitable for X-ray diffraction studies were successfully grown through slow diffusion of hexane into their chloroform solutions. Single-crystal data were collected on a Bruker SMART CCD diffractometer (Mo $K\alpha$ radiation and λ = 0.71073 Å) in Φ and ω scan modes at 293 K. The molecular structure was solved by direct methods followed by difference Fourier syntheses and then refined by full-matrix least-squares techniques against F^2 using the SHELXL-9720 program.³⁴ The positions of hydrogen atoms were calculated and refined isotropically using a riding model. All other non-hydrogen atoms were refined isotropically. Absorption corrections were applied using SADABS.³⁵

Computational Details. DFT calculations were conducted with the B3LYP method for all of the iridium(III) complexes. The 6-31G(d,p) basis set was applied for C, H, N, O, F, and Se atoms, while effective core potentials employed for Ir atoms were a LanL2DZ basis set.^{36,37} Excitation behaviors were acquired by TD-DFT calculations

on the basis of the optimized ground state geometries. Additionally, the natural transition orbital (NTO) based on the first triplet state (T_1) geometries optimized by UB3LYP was analyzed for $S_0 \rightarrow T_1$ excitation. All of the calculations were performed using the Gaussian 09 program.³⁸

RESULTS AND DISCUSSION

Synthesis and Characterization. Synthetic protocols of the organic ligands and the asymmetric ppy-type Ir(III) phosphorescent complexes are shown in Schemes 1 and 2, respectively. The ligand L-Se can be easily prepared by Stille cross-coupling between 2-(tributylstannyl)pyridine and 2-bromoselenophene prepared by the bromination of selenophene with NBS. For synthesis of the ligands with an aryl selenide unit, the key intermediate diselenide Br-2Se has to be prepared by the reaction between 4-bromiodobenzene and selenium powder according to the reported literature (Scheme 1).³⁹ The diaryl selenones Br-SeO-0F–Br-SeO-3F have been synthesized by two successive steps. First, Br-2Se was coupled with the corresponding arylboronic acid with nano CuO as catalyst (Scheme 1).⁴⁰ Second, the CuO catalyst was removed by filtration and the solvent was evaporated. The residue was dissolved in CHCl_3 , and *m*-chloroperbenzoic acid (mCPBA) was added at room temperature. After the diaryl selenones were obtained, they were coupled with 2-(tributylstannyl)pyridine, respectively, to give the ligand precursors L-SeO-0F–L-SeO-3F, which were reduced by hydrazine hydrate into the target ligands L-Se0F–L-Se3F with an aryl selenide unit (Scheme 1). In addition, these organic ligands can also be prepared by the strategy developed by Ranu's group.⁴¹ In order to enhance the EI/ET ability of the concerned Ir(III) phosphorescent complexes, a fluorine group has been introduced to balance the HI/HT ability and bring enhanced EL performance.

Clearly, it should be more convenient to obtain the target ligands L-Se0F–L-Se3F through Stille cross-coupling between 2-(tributylstannyl)pyridine and the corresponding brominated aryl selenide (Scheme S1 in the Supporting Information) without both the oxidation of the brominated aryl selenides and the reduction of the ligand precursors (Scheme 1). Unfortunately, the protocol in Scheme S1 involves two drawbacks. First, it was hard to purify the brominated aryl selenides by column chromatography due to their polarity being very similar to that of the impurities. Second, the yield of the Stille coupling between 2-(tributylstannyl)pyridine and the brominated aryl selenides was very low (<20%). This might be ascribed to the electron-donating selenium atom in the brominated aryl selenides passivating the bromine group in the concerned aryl selenides. In contrast, the bromine groups in the diaryl selenones are much more active in the mechanism of the Stille cross-coupling reaction.^{42–44}

All the obtained ligands have been characterized by ^1H , ^{13}C , and ^{19}F NMR spectra. In the ^1H NMR spectrum of L-Se1F, the doublet resonance peak at 8.68 ppm can be safely assigned to the aromatic proton linked to the C atom next to the N atom in the pyridine ring, the doublet of doublets resonance peak at 7.88 ppm should be attributed to the two aromatic protons linked to the C atoms adjacent to the C atom bonded with a pyridyl unit in the phenyl ring of ppy, the triplet of doublets resonance peak at 7.74 ppm should be attributed to the aromatic proton linked to the C atom at the para position of the N atom in the pyridine ring, the doublet of triplets resonance peak at 7.69 ppm should be ascribed to the aromatic

proton bonded with the C atom adjacent to the C atom bonded with the phenyl unit in the pyridine ring, the multiplet resonance peaks located in the range of 7.54–7.50 ppm can be assigned to two aromatic protons attached to the C atoms at the meta position of the fluorinated C atom in the pendant phenyl ring, the doublet of triplets resonance peak at 7.48 ppm should be attributed to two aromatic protons linked to the C atoms at the ortho position of the C atom bonded with the Se atom in the phenyl unit of ppy, and the doublet of doublets resonance peak at 7.23 ppm should be assigned to the aromatic proton attached to the C atom at the para position of the C atom bonded with the phenyl unit in the pyridine ring of ppy. The triplet of triplets resonance peak at 7.01 ppm should be assigned to the two aromatic protons linked to the C atoms at the ortho position of the fluorinated C atom in the pendant phenyl ring. In the ^1H NMR spectrum of L-Se, the doublet resonance peak at 8.53 ppm can be safely assigned to the aromatic proton linked to the C atom next to the N atom in the pyridine ring, the doublet of doublets resonance peak at 8.05 ppm should be attributed to the aromatic proton linked with the C atom adjacent to the C atom bonded with the pyridyl unit in the selenophene ring of L-Se, and the doublet of doublets resonance peak at 7.13 ppm should be ascribed to the aromatic proton linked to the C atoms at the meta position of the C atom bonded with the pyridyl unit in the selenophene ring of L-Se. A full assignment of resonance signals observed for ^1H NMR spectra of other obtained ligands is shown in Figure S1.

After the organic ligands were obtained, metalation of the corresponding cyclometalating ligand (L-Se0F/L-Se1F/L-Se2F/L-Se3F) and cyclometalating ligand L-Se with $\text{IrCl}_3 \cdot n\text{H}_2\text{O}$ yielded the colored cyclometalated Ir(III) μ -chloro-bridged dimers (Scheme 2). Then, the dimers were converted into the designed asymmetric Ir(III) phosphorescent complexes by mixing the corresponding μ -chloro-bridged dimer with Tl(acac) in CH_2Cl_2 at room temperature. The synthetic approach based on the reaction of $\text{IrCl}_3 \cdot n\text{H}_2\text{O}$ with equimolar amount of two different cyclometalating ligands should result in the formation of a statistical mixture of one heteroleptic $[\text{Ir}(\text{N}^{\wedge}\text{C}_1)(\text{N}^{\wedge}\text{C}_2)(\text{acac})]$ complex and two homoleptic $[\text{Ir}(\text{N}^{\wedge}\text{C})_2(\text{acac})]$ complexes.^{45,46} Except for the target asymmetric heteroleptic complexes with two different ppy-type ligands, two symmetric heteroleptic complexes with the same ppy-type ligands have been observed as well. The symmetric heteroleptic complex with aromatic selenophene groups (Ir-Se) is obtained with reaction yields in the range of 20.3–24.1%, while another kind of symmetric heteroleptic complex with aromatic selenide groups appears with reaction yields in the range of 19.8–23.3%. The overall yields for both the asymmetric heteroleptic Ir(III) complex and two symmetric heteroleptic Ir(III) complexes are in the range of 67.5–72.4%. The emerging statistical mixture of this synthetic approach is obviously not beneficial to enhance the reaction yields in terms of the target asymmetric heteroleptic Ir(III) complexes. Effective synthetic approaches still need to be explored. All of the asymmetric Ir(III) complexes and their symmetric heteroleptic parent complex Ir-Se have been characterized by ^1H , ^{13}C , and ^{19}F NMR spectra. In the ^1H NMR spectra for all the asymmetric complexes, two sets of doublet resonance peaks located at ca. 8.50 and 8.20 ppm have been observed for the two aromatic protons linked to the C atoms next to the N atoms in the two pyridine rings of the two different ppy-type ligands, respectively. The resonance signals at ca. 1.80 ppm

assigned to the two methyl groups in the acetylacetonate auxiliary ligands of these Ir(III) phosphorescent complexes split into two singlet peaks as well. However, only one resonance peak was detected for these aforementioned protons in the traditional heteroleptic Ir(III) complexes with two identical cyclometalating ppy-type ligands.³

In the ¹H NMR spectra for their symmetric heteroleptic parent complex **Ir-Se**, only one doublet resonance peak located at 8.32 ppm has been observed for two aromatic protons linked to the C atoms next to the N atoms in the two pyridine rings in the two ligands **L-Se**. Meanwhile, only one doublet resonance peak located at 6.33 ppm has been observed for the two aromatic protons bonded with the C atoms adjacent to the C atoms coordinating to Ir atoms in the selenophene rings of the two ligands **L-Se**. Two singlet resonance peaks at 5.22 and 1.81 ppm can be safely ascribed to the acetylacetonate auxiliary ligands. In the ¹H NMR spectrum for **Ir-Se1F**, two sets of doublet resonance peaks located at 8.46 and 8.13 ppm have been observed for the aromatic protons attached to the C atom next to the N atoms in **L-Se1F** and that in **L-Se**, respectively. The multiplet resonance peaks located in the range of 7.78–7.76 ppm can be assigned to the aromatic proton linked to a C atom adjacent to the Se atom in the ligand **L-Se** and the aromatic proton attached to the C atom next to the C atom bonded with the phenyl unit in the pyridine ring of **L-Se1F**, respectively. The triplet of doublets resonance peak at 7.69 ppm should be ascribed to the aromatic proton attached to the C atom at the para position of the N atom in the pyridine ring of **L-Se1F**. The triplet of doublets resonance peak at 7.52 ppm should be attributed to the aromatic proton linked to the C atom at the para position of the N atom in the pyridine ring of **L-Se**, while the doublet resonance peak at 7.35 ppm should be ascribed to the aromatic proton linked to the C atom adjacent to the C atom bonded with the selenophene unit in **L-Se**. The multiplet resonance peaks located in the range of 7.33–7.28 ppm can be assigned to the aromatic proton linked to the C atom at the meta position of the C atom coordinating to the Ir atom and two aromatic protons bonded with the C atoms at the meta position of the fluorinated C atom in **L-Se1F**, respectively. Induced by the proton on the pyridine ring in **L-Se1F**, the triplet of doublets resonance peak at 7.10 ppm should be assigned to the proton attached to the C atom at the para position of the C atom bonded with the phenyl unit. The triplet resonance peak at 6.87 ppm should be assigned to the two aromatic protons linked to the C atoms at the ortho position of the fluorinated C atom in **L-Se1F**. The multiplet resonance peaks located in the range of 6.83–6.78 ppm can be assigned to one aromatic proton linked to the C atom at the para position of the C atom coordinating to the Ir atom in **L-Se1F** and one aromatic proton bonded with the C atom at the para position of the C atom bonded with the selenophene unit in the pyridine ring of **L-Se**, respectively. Two sets of doublet resonance peaks located at 6.22 and 6.03 ppm have been observed for the aromatic protons linked to the C atom adjacent to the C atom coordinating to the Ir atom in **L-Se** and that in **L-Se1F**, respectively. The singlet resonance signals at 5.20 ppm can be safely ascribed to the proton linked to the C atoms adjacent to the two carbonyl groups in the acetylacetonate after coordinating to the Ir atom, while two singlet resonance peaks at 1.79 and 1.78 ppm can be assigned to the two methyl groups in the acetylacetonate auxiliary ligand. Full assignment of the ¹H NMR signals for other asymmetric heteroleptic Ir(III) complexes is shown in Figure

S4. In the ¹⁹F NMR spectra for **Ir-Se1F** and **Ir-Se2F**, only singlet resonance signals at –114.20 and –109.50 ppm can be found. In contrast, **Ir-Se3F** can show two sets of peaks with 2:1 peak area ratio for the doublet peak at –133.50 ppm and the triplet peak at –161.30 ppm due to the F–F coupling. All of these ¹⁹F NMR results clearly indicate the expected substitution pattern of the fluorine groups in these asymmetric heteroleptic Ir(III) complexes. In the ¹³C NMR spectrum of **Ir-Se1F**, the doublet resonance peak at 162.44 ppm induced by F–C coupling with $J_{FC} = 245.3$ Hz can be safely assigned to the aromatic carbon linked with an –F group and the doublet resonance peak at 136.68 ppm induced by F–C coupling with $^3J_{FC} = 7.9$ Hz can be safely assigned to the aromatic carbon at a position ortho to the Se atom in the pendant phenyl of **L-Se1F**. Meanwhile, the doublet resonance peak at 124.29 ppm induced by F–C coupling with $^4J_{FC} = 3.1$ Hz can be safely ascribed to the aromatic carbon attached to an Se atom and the doublet resonance peak at 116.30 ppm induced by F–C coupling with $^2J_{FC} = 21.4$ Hz can be safely ascribed to an aromatic carbon at a position ortho to the fluorinated atom in **L-Se1F**. For **Ir-Se2F**, the doublet of doublets resonance peak located at 162.73 ppm due to F–C coupling with $J_{FC} = 249.9$ Hz has been observed for the two aromatic carbons linked with an –F group and the triplet resonance peak located at 135.01 ppm with $^3J_{FC} = 8.9$ Hz should be attributed to the aromatic carbon bonded with an Se atom. The doublet of doublets resonance peak at 114.69 ppm induced by F–C coupling with $^2J_{FC} = 19.0$ Hz can be safely assigned to the aromatic carbon at a position ortho to the Se atom in **L-Se2F** and the triplet resonance peak at 102.23 ppm induced by F–C coupling with $^2J_{FC} = 25.2$ Hz can be safely ascribed to the aromatic carbon between the two aromatic carbon atoms bonded with an –F group. The ¹³C NMR spectrum for **Ir-Se3F** shows a doublet of doublets resonance peak at 150.86 ppm induced by F–C coupling with $J_{FC} = 251.8$ Hz assigned to the two fluorinated aromatic carbons at a position meta to the Se atom in **L-Se3F**, while the doublet of triplets resonance peak at 139.11 ppm induced by F–C coupling with $J_{FC} = 249.7$ Hz can be attributed to a fluorinated aromatic carbon at a position para to the Se atom in **L-Se3F**. Meanwhile, the doublet of doublets resonance peak located at 125.26 ppm due to F–C coupling with $^3J_{FC} = 12.1$ Hz has been observed for the aromatic carbon linked to an Se atom and the doublet of doublets resonance peak located at 117.71 ppm due to F–C coupling with $^2J_{FC} = 16.2$ Hz should be attributed to the aromatic carbon at a position ortho to the Se atom in **L-Se3F**. When the results of their ¹⁹F NMR spectra are combined with those of ¹³C NMR spectra, the structures of these asymmetric heteroleptic Ir(III) complexes have been properly confirmed. In addition, **L-SeO-0F–L-SeO-3F** have also been employed to synthesize asymmetric heteroleptic Ir(III) complexes with **L-Se** with the aim to take advantage of the electronic features of the aromatic selenone group (–SeO₂Ar). Unexpectedly, the selenone group (–SeO₂Ar) had been transferred into the selenide unit (–SeAr) and just **Ir-Se0F–Ir-Se3F** were obtained. On the basis of all the results (Scheme S2 and Table S1), it can be safely concluded that the selenone group in the synthesis of these asymmetric complexes has been mainly reduced by the solvent mixture THF/H₂O with IrCl₃·*n*H₂O as catalyst. Also as a catalyst, the dimer formed in the first step can contribute to the reduction of the selenone group in the synthesis of these asymmetric Ir(III) complexes as well.

Single-Crystal X-ray Crystallography. The single crystals of Ir-Se2F and Ir-Se3F with high quality have been successfully obtained through slow diffusion of hexane into their chloroform solutions. Their structures were determined by single-crystal X-ray crystallography (Figure 1). Detailed data

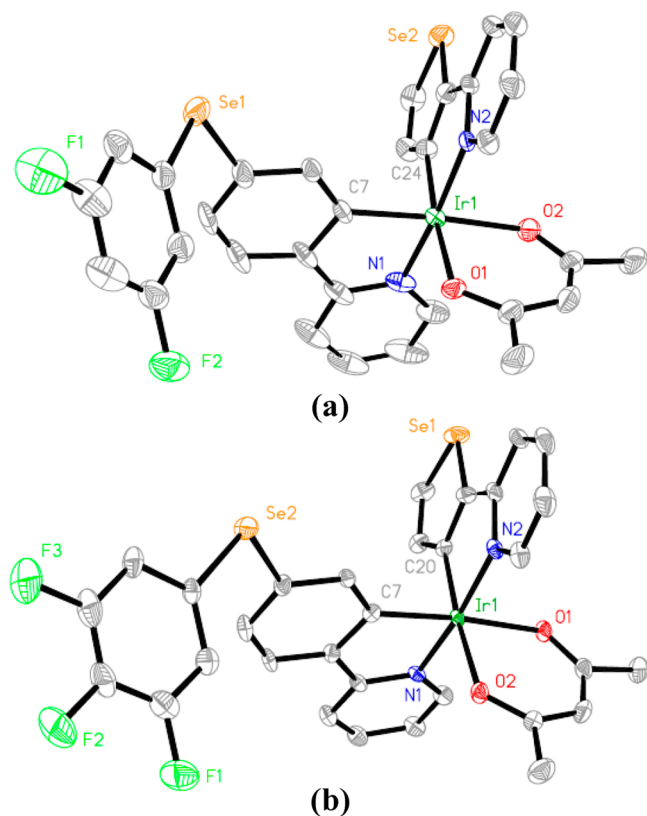


Figure 1. Perspective views of (a) Ir-Se2F and (b) Ir-Se3F with thermal ellipsoids are drawn at the 30% probability level. All hydrogen atoms are omitted for clarity.

of each structure are given in Table 1 as well as Tables S2 and S3. In their single crystals, the molecules of both Ir-Se2F and Ir-Se3F pack in the same space group $P\bar{1}$ to form a triclinic crystal system (Table 1). As depicted in Figure 1, two ppy-type ligands and one acetylacetonate anion around the Ir center furnish a slightly distorted octahedral chelating skeleton with *cis*-C,C, *cis*-O,O, and *trans*-N,N chelating disposition for Ir-Se2F and Ir-Se3F. For Ir-Se2F, the N1–Ir1–N2, O1–Ir1–C24, and O2–Ir1–C7 bond angles are 174.3(3)°, 173.2(3)°, and 174.9(3)°, while those for Ir-Se3F are 173.3(17)°, 174.06(18)°, and 174.08(18)°, respectively. The Ir–C, Ir–N, and Ir–O bond lengths are similar to those of our previously reported asymmetric heteroleptic Ir(III) complexes.^{31–33} The C–Se–C bond angles in the aryl selenide units are 99.2(4)° for Ir-Se2F and 101.6(2)° for Ir-Se3F, which are less than the theoretical 109.5° due to the electrostatic repulsion between the unshared pair electrons on selenium atoms and the bonding electrons of the Se–C bonds. In their analogous complexes with aromatic ether and aromatic sulfide units, the C–O–C (ca. 104°) and C–S–C (ca. 120°) bond angles are larger than that of C–Se–C in the aryl selenide units of these asymmetric heteroleptic Ir(III) complexes.⁷ The C–Se–C bond angles in the aryl selenophene units are 86.2(4)° for Ir-Se2F and 85.6(3)° for Ir-Se3F, similar to the reported data.⁴⁷ In their analogous scaffolds with thiophene¹⁸ and tellu-

ophene⁴⁷ units, the C–S–C bond angles in thiophene units and C–Te–C bond angles in tellurophene units are ca. 90 and 80°, respectively. The bond lengths in the selenophene units for Ir-Se2F and Ir-Se3F are ca. 1.86 Å, similar to the reported data,⁴⁷ while those in the thiophene and tellurophene units are 1.73 and 2.10 Å, respectively.

Thermal and Photophysical Properties. The thermal properties of these asymmetric heteroleptic Ir(III) complexes have been examined with thermogravimetric analysis (TGA) and different scanning calorimetry (DSC) under a nitrogen flow. The TGA results reveal their thermal stability with decomposition temperatures (T_d) ranging from ca. 280 to 290 °C (Table S4 and Figure S17), similar to that of their parent complex Ir-Se. The DSC traces have indicated their glass-transition temperature (T_g) in the range from ca. 110 to 115 °C (Table S4 and Figure S16).

In their UV–vis spectra (Figure 2a), the high-energy absorption bands before ca. 370 nm can be safely assigned to the π – π^* transition of the two ppy-type ligands.⁴⁸ On the basis of the results of time-dependent density functional theory (TD-DFT) calculations, the characters of their $S_0 \rightarrow S_1$ transitions corresponding to the major absorption bands can be represented by their HOMO \rightarrow LUMO (H \rightarrow L) transitions due to their large contribution of over 95% (Table 3). Hence, on the basis of the H \rightarrow L transition features of these asymmetric heteroleptic Ir(III) complexes, their major absorption bands should exhibit ligand to ligand charge transfer (LLCT) features from the π orbitals of the ppy-type ligand with the selenophene unit to the π^* orbitals of the ppy-type ligand with the selenide group, while the Ir–(ppy)₂(acac)-type complexes typically show intraligand charge transfer (ILCT) features in their absorption bands from the phenyl π orbitals to the pyridyl π^* orbitals in the ppy-type ligand.^{2,7} In addition, obvious metal to ligand charge transfer (MLCT) features from the Ir(III) center to the π^* orbitals of the ppy-type ligand with a selenide group can be involved in the weak singlet-state absorption bands between 370 and 450 nm (Figure 2a) of these asymmetric heteroleptic Ir(III) complexes. The weak triplet-state absorption bands with the lowest energy after 450 nm should be mainly induced by the $^3\pi$ – π^* transition of the ppy-type ligand L-Se with the selenophene ring together with some 3 MLCT transition characters from the Ir(III) center to the π^* orbitals of the pyridyl ring in the ligand L-Se (Figure 3 and Table 3). These asymmetric heteroleptic Ir(III) complexes show almost identical absorption spectra in the visible-light region (Figure 2a) with sequential introduction of electron-withdrawing fluorine substituents to the selenide groups, mainly due to the negligible contribution of the fluorinated phenyl ring to both HOMO and LUMO orbitals as well as the HOMO \rightarrow LUMO (H \rightarrow L) transition (Figure 3) on the basis of the results of time-dependent density functional theory (TD-DFT) calculations.

The excitation spectra of these heteroleptic Ir(III) complexes have been measured with a monitoring wavelength at ca. 580 nm in CH₂Cl₂ solution and at ca. 584 nm in doped CBP films at 293 K (Figures S10 and S11 and Table 2). It has been found that the excitation spectra are quite similar to the absorption spectra (Figure 2a) at 293 K. All of these heteroleptic Ir(III) complexes show almost identical spectral lines in their excitation features and similar maximum excitation wavelengths located at ca. 338 nm. Increasing the number of –F substituents on the selenide groups has nearly

Table 1. Crystal and Data Parameters for Structures Ir-Se2F and Ir-Se3F

	Ir-Se2F	Ir-Se3F
CCDC no.	1819886	1819887
formula	C ₃₁ H ₂₃ F ₂ IrN ₂ O ₂ Se ₂	C ₃₁ H ₂₂ F ₃ IrN ₂ O ₂ Se ₂
formula wt	843.63	861.62
cryst syst	triclinic	triclinic
space group	$P\bar{1}$	$P\bar{1}$
<i>a</i> (Å)	8.6268(4)	8.3973(7)
<i>b</i> (Å)	12.1741(7)	12.3883(9)
<i>c</i> (Å)	14.3748(8)	14.2705(11)
α (deg)	99.161(5)	100.594(2)
β (deg)	101.247(4)	102.471(2)
γ (deg)	103.133(4)	95.113(2)
<i>V</i> (Å ³)	1408.86(14)	1411.91(19)
<i>Z</i>	2	2
<i>D</i> _{calcd} (g nm ⁻³)	1.989	2.207
cryst size (mm ³)	0.400 × 0.100 × 0.050	0.200 × 0.150 × 0.100
<i>F</i> (000)	804	820
μ (mm ⁻¹)	12.514	7.359
θ range (deg)	4.43–73.27	2.48–27.50
no. of diffn reflns	10041	35207
total no. of rflns	5504	6446
no. of params	363	372
R1, wR2 (<i>I</i> > 2.0 σ (<i>I</i>)) ^a	0.0440, 0.1112	0.0390, 0.1009
R1, wR2 (all data)	0.0549, 0.1226	0.0474, 0.1053
GOF on <i>F</i> ^{2b}	0.765	1.012

$$^a R1 = \sum ||F_o| - |F_c|| / \sum |F_o|. \quad wR2 = \{ \sum [w(F_o^2 - F_c^2)^2] / \sum [w(F_o^2)^2] \}^{1/2}. \quad ^b GOF = [(\sum w|F_o| - |F_c|)^2 / (N_{obs} - N_{param})]^{1/2}.$$

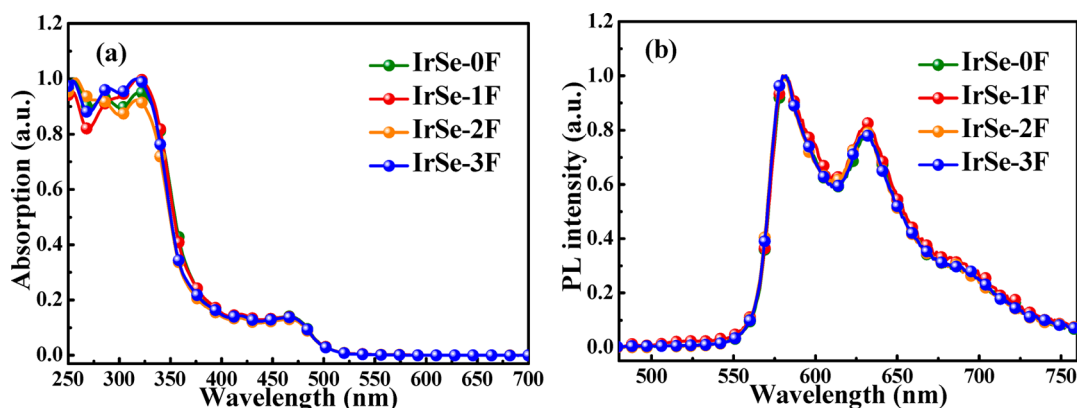


Figure 2. (a) UV-vis absorption spectra and (b) photoluminescence (PL) spectra of the asymmetric heteroleptic Ir(III) complexes in CH₂Cl₂ solution recorded at 293 K.

no effect on their excitation features, which is due to the fact that the fluorinated phenyl rings make almost no contribution to the composition of HOMO and LUMO orbitals and NTOs (Figures 3 and 4) on the basis of the results of the TD-DFT calculations.

Photoluminescent (PL) spectra of these heteroleptic Ir(III) complexes have been measured in CH₂Cl₂ solution at 293 K. Under irradiation with 360 nm UV light, all of these heteroleptic Ir(III) complexes emit an orange-red phosphorescent band at ca. 580 nm accompanied by a slightly weaker band at ca. 631 nm and a shoulder peak at ca. 691 nm (Figure 2b and Table 2), while their symmetric parent complex Ir-Se shows a bathochromic shift in the emission color with an orange-red phosphorescent band at 586 nm accompanied by a slightly weaker band at 633 nm and a shoulder peak at 700 nm. All of the heteroleptic Ir(III) complexes show a very high Φ_p value of ca. 0.9, much higher than that of their symmetric

parent complex Ir-Se (Φ_p ca. 0.6), indicating the advantage of their chemical structures in furnishing high Φ_p . These observations demonstrate that the design strategy of the asymmetric heteroleptic Ir(III) complexes can finely tune the emission wavelength and Φ_p .^{30,32} They share nearly identical spectral lines for their phosphorescence signals in both CH₂Cl₂ solution and doped CBP films (Figure 2b and Figures S9 and S12). The PL emission intensity of the emission band around 584 nm in doped CBP films is markedly enhanced in comparison with that in CH₂Cl₂ solution, while the PL emission intensity of the emission band around 631 nm in doped CBP films is significantly reduced and the PL emission intensity of the emission band around 691 nm in doped CBP films almost disappears. These results may be due to variation of the vibration mode of the excited Ir(III) complexes in the rigid matrix of CBP films. In addition, the Ir(ppy)₂(acac)-type complexes generally exhibit a featureless emission spectrum

Table 2. Photophysical of the Asymmetric Heteroleptic Ir(III) Complexes and Their Parent Complex Ir-Se

	absorption (293 K) ^a λ_{abs} (nm)	excitation (293 K) ^b λ_{max} (nm)	emission (293 K) ^c λ_{em} (nm)	$\Phi_{\text{p}}^{\text{d}}$ (%) degassed/aerated	$\tau_{\text{p}}^{\text{e}}$ (μs) degassed/aerated
Ir-Se0F	256 (4.18), 285 (4.15), 319 (4.16), 418 (3.35), 466 (3.33)	338 (580)	580, 631, 690 ^{sh}	91.23/3.65	3.99/0.23 (580)
Ir-Se1F	254 (4.38), 288 (4.36), 318 (4.40), 418 (3.57), 466 (3.54)	337 (580)	580, 631, 691 ^{sh}	93.09/3.94	3.81/0.21 (580)
Ir-Se2F	258 (4.54), 285 (4.50), 317 (4.50), 416 (3.67), 465 (3.65)	337 (581)	581, 632, 691 ^{sh}	90.14/3.42	3.86/0.22 (581)
Ir-Se3F	254 (4.48), 290 (4.47), 317 (4.48), 418 (3.64), 466 (3.62)	339 (581)	581, 632, 692 ^{sh}	93.21/4.16	4.16/0.24 (581)
Ir-Se	256 (4.07), 282 (4.17), 307 (4.22), 371 (3.77), 423(3.56), 479(3.59)	338 (586)	586, 633, 700 ^{sh}	60.32/2.03	3.93/0.24 (586)

^aMeasured at a concentration of ca. 10^{-5} M in CH_2Cl_2 , with $\log \epsilon$ values given in parentheses. sh: shoulder. ^bMeasured at a concentration of ca. 10^{-5} M in CH_2Cl_2 . λ_{max} represents the excitation wavelength at which the maximum emission intensity of the monitoring wavelength was obtained. The monitoring wavelength is shown in parentheses (in nm). ^cMeasured at a concentration of ca. 10^{-5} M in CH_2Cl_2 , with λ_{ex} 400 nm. ^dRelative to *fac*-[Ir(ppy)₃] ($\Phi_{\text{p}} = 0.97$) in CH_2Cl_2 solution, with λ_{ex} 360 nm. ^eMeasured at a sample concentration of ca. 10^{-5} M in CH_2Cl_2 solution at 293 K. The monitoring wavelength is provided in parentheses (in nm).

Table 3. TD-DFT Results of These Asymmetric Heteroleptic Ir(III) Complexes on the Basis of Their Optimized S₀ Geometries

complex	MO	contribution of metal d _π orbitals and π orbitals of ligand to MOs (%)				main confign of S ₀ → S ₁ excitation, E _{cal} (eV)/ λ_{cal} (nm)/ <i>f</i> ^a	main confign of S ₀ → T ₁ excitation/, E _{cal} (eV), λ_{cal} (nm) ^a
		Ir	L-Se	L-Se0F	acac		
Ir-Se0F	L+1	6.52	82.12	9.05	2.31	H → L (96.73), 2.595, 477.7, 0.0239	H → L+1 (77.54), 2.201, 563.32
	L	4.49	3.56	90.35	1.60		
	H	48.88	34.73	12.01	4.38		
	H-1	3.88	0.73	93.88	1.51		
Ir-Se1F	L+1	6.58	80.06	11.08	2.28	H → L (95.82), 2.672, 464.0, 0.0319	H → L+1 (73.74), 2.192, 565.7
	L	4.66	5.51	88.04	1.80		
	H	48.28	32.72	14.70	4.30		
	H-1	14.42	6.50	72.09	6.99		
Ir-Se2F	L+1	6.48	81.80	9.35	2.37	H → L (96.97), 2.555, 485.2, 0.0213	H → L+1 (77.52), 2.205, 562.3
	L	4.44	3.22	90.75	1.59		
	H	48.06	36.35	11.03	4.56		
	H-1	39.95	6.96	20.15	32.94		
Ir-Se3F	L+1	6.48	81.78	9.37	2.37	H → L (97.02), 2.547, 486.7, 0.0198	H → L+1 (77.99), 2.207, 561.8
	L	4.38	3.07	90.99	1.56		
	H	47.92	37.01	10.56	4.51		
	H-1	38.45	6.38	23.09	32.08		

^aH→L denotes the transition from the HOMO to LUMO. E_{cal}, λ_{cal} , and *f* denote the calculated excitation energy, calculated emission wavelength, and oscillator strength, respectively. The oscillator strength of S₀ → T₁ is zero owing to the spin-forbidden character of the singlet–triplet transition under TD-DFT calculations in the Gaussian program with no consideration of spin–orbital coupling.

with a predominant ³MLCT emission feature, while these asymmetric complexes display structured phosphorescent spectra in both CH_2Cl_2 solution and doped CBP films, especially for the major emission bands (Figure 2b and Figures S9 and S12).^{3,7} In order to interpret the phosphorescent feature, i.e. T₁ state character of these asymmetric heteroleptic Ir(III) complexes, natural transition orbital (NTO) analysis has been conducted for their S₀ → T₁ excitations on the basis of the optimized T₁ geometries.

From the distribution patterns of the NTO hole and particle orbitals for all of these asymmetric heteroleptic Ir(III) complexes, it can be seen clearly that they all display a predominant ligand-centered feature, centering on the ligand L-Se due to its large contribution to the NTOs (Figure 4 and Table 4). This outcome might be ascribed to the electron-rich

features associated with the selenophene unit to facilitate the electron transition process. Due to the slight contribution of L-Se0F–L-Se3F to the NTOs of Ir-Se0F–Ir-Se3F, sequential introduction of electron-withdrawing fluorine substituents to the selenide groups has nearly no effect on their NTO distribution (Figure 4). This may account for the nearly identical emission spectra for these asymmetric heteroleptic Ir(III) complexes. Thus, we can conclude that ligand-centered ³ π – π^* dominates the character of the T₁ state of all the asymmetric heteroleptic Ir(III) complexes. On the basis of the reported photophysical results for phosphorescent complexes,^{49–51} the ligand-centered ³ π – π^* features of the T₁ state typically may display vibronic progressions in the phosphorescent spectra. As a result, structured line profiles

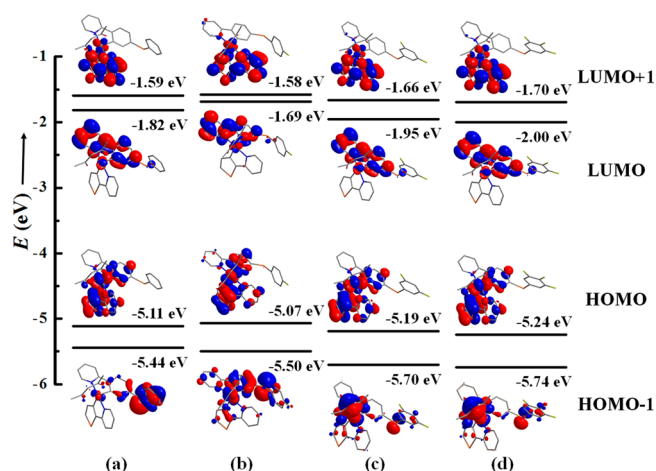


Figure 3. Molecular orbital (MO) patterns (isocontour value 0.030) of the asymmetric heteroleptic Ir(III) complexes on the basis of their optimized S_0 geometries: (a) Ir-Se0F; (b) Ir-Se1F; (c) Ir-Se2F; (d) Ir-Se3F.

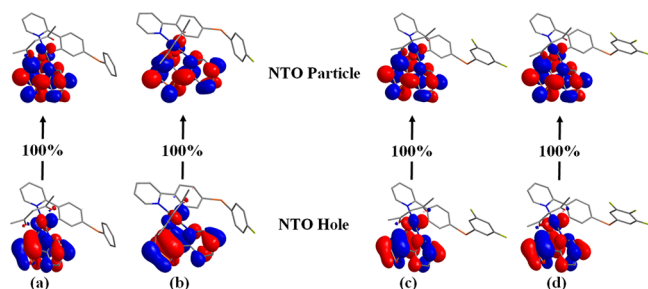


Figure 4. Natural transition orbital patterns (isocontour value 0.030) for $S_0 \rightarrow T_1$ excitation for these heteroleptic Ir(III) complexes on the basis of their optimized T_1 geometries: (a) Ir-Se0F; (b) Ir-Se1F; (c) Ir-Se2F; (d) Ir-Se3F.

Table 4. NTO Results for the Heteroleptic Ir(III) Complexes on the Basis of Optimized T_1 Geometries

complex	NTO ^a	contribn of metal d_x orbitals and π orbitals of ligand to NTOs (%)			
		Ir	L-Se	L-OF	acac
Ir-Se0F	H	22.61	72.86	3.12	1.41
	P	7.33	82.66	8.00	2.01
Ir-Se1F	H	23.00	71.93	3.65	1.42
	P	7.44	82.46	8.06	2.04
Ir-Se2F	H	22.07	73.73	2.77	1.43
	P	7.32	83.00	7.59	2.09
Ir-Se3F	H	21.88	73.97	2.74	1.41
	P	7.33	82.98	7.61	2.08

^aH and P denote NTO hole and particle orbitals, respectively.

measured in CH_2Cl_2 solution at 293 and 77 K as well as in 8 wt % doped CBP films have been obtained for the phosphorescent bands of all these asymmetric heteroleptic Ir(III) complexes (Figure 2b and Figures S9 and S12). The emission bands around 581, 631, and 691 nm can be assigned to the transfer of 0–0, 0–1, and 0–2 vibronic states, respectively. In order to interpret the emission fine structure of these

asymmetric heteroleptic Ir(III) complexes, infrared (IR) spectroscopic investigations were carried out, and the IR spectra are almost identical (Figure S19). Vibrations at ca. 1570 and ca. 1510 cm^{-1} can be assigned to C=O and C=C stretching modes, respectively. There are many vibrations in the region between 1250 and 1500 cm^{-1} , including symmetric and asymmetric vibrations. The two intense vibration bands at ca. 1469 and 1390 cm^{-1} can be ascribed to the C–C stretching mode in the aromatic systems of the two different ppy-type ligands. The emission bands in the PL spectra at 77 K (Table S4 and Figure S9) of these asymmetric heteroleptic Ir(III) complexes show two vibronic spacings (from ca. 576 to 627 nm and from ca. 627 to 690 nm) around ca. 1410 and 1430 cm^{-1} , respectively. Thus, the vibronic spacings in the emission bands are similar to vibration frequencies in the aromatic systems. These outcomes should be able to further account for the ligand-centered $^3\pi-\pi^*$ character of the T_1 state of all the asymmetric heteroleptic Ir(III) complexes. In addition to the dominant $^3\pi-\pi^*$ features, the T_1 state of all the asymmetric heteroleptic Ir(III) complexes should possess some MLCT features by considering the difference in contributions from the Ir(III) center to the NTO hole and particle orbitals (Table 4). This result should account for the structureless spectral line profile at the long-wavelength region in the phosphorescent spectra of all the asymmetric heteroleptic Ir(III) complexes (Figure 2b). Clearly, there is good consistency between experimental and theoretical results, indicating the validity of the employed theoretical strategies. From the structured pattern of the PL spectra of the parent complex Ir-Se (Figure S8), it can be concluded that the T_1 state of Ir-Se also dominantly shows the $^3\pi-\pi^*$ feature of the L-Se ligand. Hence, Ir-Se can exhibit phosphorescent wavelength and spectral pattern very similar to those of the asymmetric heteroleptic Ir(III) complexes (Table 2, Figure 2b, and Figure S8).

The emission lifetimes of all these asymmetric heteroleptic Ir(III) complexes in aerated and degassed CH_2Cl_2 solution are ca. 0.23 and 3.90 μs (Table 2, Figures S13 and S14), respectively, while their lifetimes in 8 wt % doped CBP films are ca. 3.10 μs (Table S4 and Figure S15). The lifetimes in degassed CH_2Cl_2 solution and in doped CBP films are enhanced by ca. 17- and 14-fold, respectively, in comparison with those in the aerated CH_2Cl_2 solution. This trend also appears in the changes of the Φ_p values for all these asymmetric heteroleptic Ir(III) complexes. Hence, the phosphorescence of all these asymmetric heteroleptic Ir(III) complexes can be significantly quenched by oxygen. However, after purging with N_2 , their Φ_p values can be enhanced by ca. 30-fold (Table 2), indicating their potential as oxygen sensors.⁵²

Electrochemical Properties. Electrochemical properties of these asymmetric heteroleptic Ir(III) complexes have been characterized in acetonitrile solution by cyclic voltammetry (CV) measurements with ferrocene (Fc) as the internal standard under a nitrogen atmosphere. In the anodic scan, all of the complexes can show a reversible oxidation wave with potential (E_{pa}) at ca. 0.40 V, while that for the parent complex Ir-Se is about 0.35 V (Table 5 and Figure S18). This oxidation potential comes from oxidation of the Ir(III) center, which is typically observed in the ppy-type Ir(III) complexes.^{7,31} Owing to the strong electron-withdrawing associated with the –F group, the reversible oxidation potential moves slightly to more positive potential region with an increase in the number of –F

Table 5. Redox Properties of the Heteroleptic Ir(III) Complexes and Their Parent Complex Ir-Se

complex	E_{pa} (V)	E_{pc} (V)	E_g (eV)		E_{HOMO} (eV) ^e	E_{LUMO} (eV) ^f
			E_g^{optc}	E_g^{cvd}		
Ir-Se0F	0.40 ^a	-2.56, ^b -2.77 ^b	2.47	2.82	-5.20	-2.38
Ir-Se1F	0.41 ^a	-2.52, ^b -2.77 ^b	2.47	2.81	-5.21	-2.40
Ir-Se2F	0.43 ^a	-2.48, ^b -2.78 ^b	2.47	2.81	-5.23	-2.42
Ir-Se3F	0.43 ^a	-2.48, ^b -2.78 ^b	2.47	2.79	-5.23	-2.44
Ir-Se	0.35 ^a	-2.62, ^b -2.84 ^b	2.42	2.77	-5.15	-2.38

^aReversible. The value was set as $E_{1/2}$. ^bIrreversible or quasi-reversible. The value was derived from the cathodic peak potential. ^cOptical energy gap E_g^{opt} calculated from the absorption onset of the UV-vis absorption spectra. ^dCV energy gap $E_g^{cv} = LUMO - HOMO$. ^eHOMO levels are calculated according to the equation $HOMO = -(4.8 + E_{pa})$ eV. ^fData are obtained from the onset potential of the first reduction wave of the CV data.

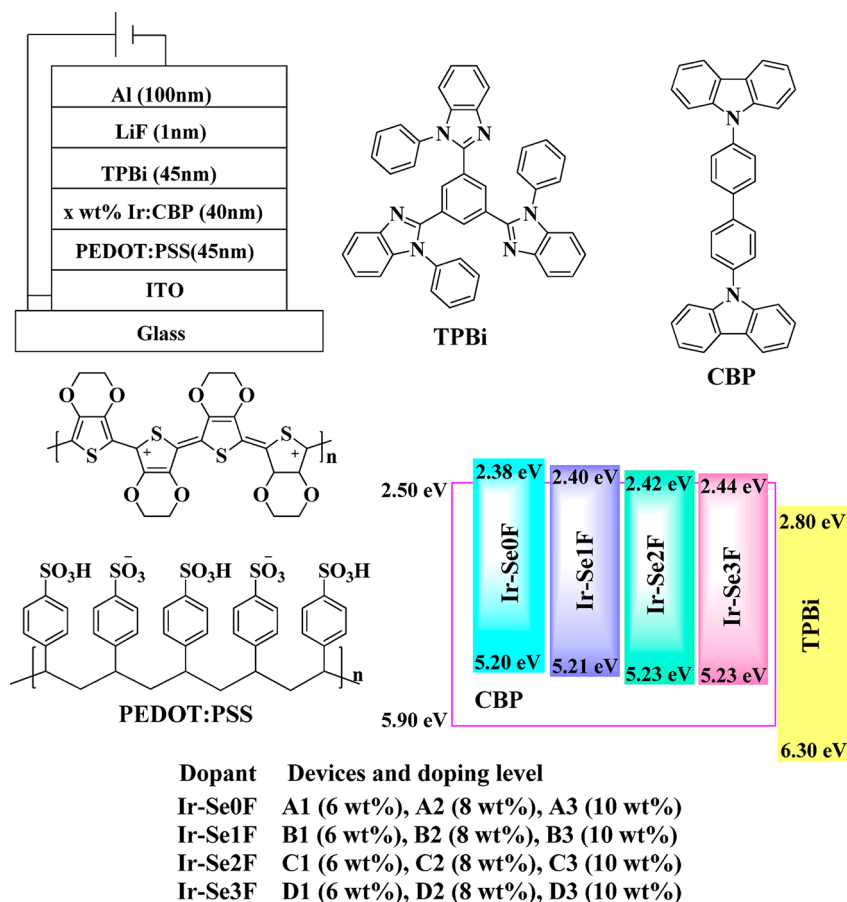


Figure 5. Device structure of the solution-processed OLEDs together with an energy level diagram and molecular structures of the materials used in the fabricated OLEDs.

substituents in the asymmetric heteroleptic Ir(III) complexes through the conjugation effect (Table 5). The electron-rich character of the two coordinating selenophene units makes the Ir(III) center in the parent complex Ir-Se more easily oxidized. Hence, Ir-Se exhibits lower oxidation potential in comparison to the asymmetric heteroleptic Ir(III) complexes (Table 5). It seems that introducing a selenophene unit can promote hole injection: i.e., the hole-trapping ability of the concerned Ir(III) complexes.

All of the asymmetric heteroleptic Ir(III) complexes also display similar reduction behavior with two irreversible reduction waves at ca. -2.50 and -2.80 V, which can be ascribed to the reduction of the pyridyl units in the organic ligands (Table 5 and Figure S18). Clearly, the -F substituents in the organic ligands with a selenide group should make the

pyridyl moieties more inclined to be reduced owing to their strong electron-withdrawing ability. As a result, more -F substituents can furnish slightly lower reduction potential to the pyridyl rings in Ir-Se1F, Ir-Se2F, and Ir-Se3F in comparison to those in Ir-Se0F and Ir-Se (Table 5). Clearly, a fluorinated selenide group can improve electron injection: i.e., the electron-trapping ability of the concerned Ir(III) complexes. Attached with two electron-rich selenophene units, the pyridyl rings in Ir-Se should be more reluctant to be reduced to furnish Ir-Se with the highest reduction potential of ca. -2.62 V (Table 5).

On the basis of the aforementioned results, the asymmetric structure of these heteroleptic Ir(III) complexes can provide the opportunity to tune the electrochemical properties of the concerned Ir(III) complexes through two different ppy-type

ligands, indicating the advantage associated with the asymmetric structure for developing new Ir(III) phosphorescent emitters.

Electroluminescent Properties. According to the literature, the EL potential for the asymmetric heteroleptic Ir(III) phosphorescent emitters with selenium-containing groups has not been explored. In addition, these asymmetric heteroleptic Ir(III) complexes possess a high Φ_p value of ca. 0.90, which is crucial for achieving high EL efficiencies.⁵³ On this basis, the EL performances of these asymmetric heteroleptic Ir(III) complexes have been characterized by simple solution-processed OLEDs with the configuration ITO/PEDOT:PSS (45 nm)/Ir *x* wt %:CBP (40 nm)/TPBi (45 nm)/LiF (1 nm)/Al (100 nm) (Figure 5). The hole injection layer (HIL) of the devices is constructed by spin-coating the solution of PEDOT:PSS. The hole-blocking and electron-transporting functions of the OLEDs are both fulfilled by the TPBi layer, while LiF serves as an electron-injection layer.

When a proper voltage is applied, all OLEDs can emit orange electrophosphorescence at ca. 584 nm (Figure 6 and

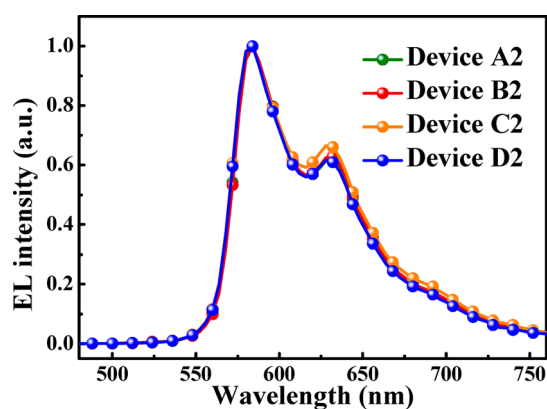


Figure 6. EL spectra for the optimized OLEDs at ca. 10 V.

Figure S21). The EL data of these solution-processed OLEDs are summarized in Table 6. As depicted in Figure 6 and Figure S21, the EL spectral line shapes for the OLEDs show a great resemblance to those of the PL spectra based on these asymmetric heteroleptic Ir(III) complexes in solution and doped CBP films (Figure 2b and Figure S12), indicating that electrophosphorescence indeed originates from the triplet states of these asymmetric heteroleptic Ir(III) complexes.

Current density–voltage–luminance characteristics and EL efficiency–luminance curves for these solution-processed OLEDs are shown in Figure 7 and 8 and Figures S21 and S22. The optimal EL efficiencies have been achieved with 8 wt % doping level of these asymmetric heteroleptic Ir(III) complexes in the emission layer of the OLEDs. All of the devices show a relatively low turn-on voltage of ca. 4.0 V (Table 6), which might benefit from the charge carrier injection/transporting ability associated with selenophene and fluorinated selenide groups. The optimized device A2 based on Ir-Se0F can show a maximum external quantum efficiency (η_{ext}) of 15.2%, a maximum current efficiency (η_L) of 49.4 cd A⁻¹, and a maximum power efficiency (η_p) of 37.0 lm W⁻¹, while the data for device B2 with Ir-Se1F as emitter are 15.8%, 50.9 cd A⁻¹, and 42.5 lm W⁻¹, respectively. (Table 6 and Figure 8a,b). In addition, device C2 with Ir-Se2F as emitter can show even higher EL efficiencies of 18.2%, 58.4 cd A⁻¹,

and 44.5 lm W⁻¹ (Table 6 and Figure 8c). Finally, the highest EL efficiencies have been achieved by device D2 based on Ir-Se3F with $\eta_{\text{ext}} = 19.9\%$, $\eta_L = 65.6$ cd A⁻¹, and $\eta_p = 57.3$ lm W⁻¹, respectively (Table 6 and Figure 8d). In addition to their attractive EL efficiencies, these solution-processed OLEDs can show high luminance over 10000 cd m⁻² at a driving voltage of less than 20 V (Table 6 and Figure 7). For the device D2 with the highest EL efficiencies, the efficiency rolloff can be maintained at ca. 12% and 25% at luminances of 100 and 1000 cd m⁻², respectively. Although -F groups on the ligand of a phosphorescent Ir(III) emitter are generally considered to be detrimental to device stability, a recent report concerning the influence of fluorination on Ir(III) complexes as phosphorescent emitters in OLEDs suggests that rational incorporation of fluorine atoms in the ligands in phosphorescent Ir(III) complexes not only can have little effect on the photophysical and thermal properties but also can fine-tune the performance of the resulting device.⁵⁴ All of these results can clearly indicate the great potential of these novel asymmetric heteroleptic Ir(III) phosphorescent emitters with both selenophene and selenide groups. Lee, Jin, et al. prepared a red-emitting *fac*-[Ir(4-phenyl-2-(selenophen-2-yl)quinoline)₃] complex with $\Phi_p = \text{ca. } 0.07$; this complex can show good EL efficiencies of 17.60%, 12.78 cd A⁻¹, and 11.46 lm W⁻¹.² Our previous green-emitting symmetric heteroleptic Ir(III) phosphorescent emitters with a diphenyl sulfide group could furnish EL efficiencies of 5.97%, 20.77 cd A⁻¹, and 12.02 lm W⁻¹.⁷ In comparison with all these EL results, the great potential of these asymmetric heteroleptic Ir(III) phosphorescent emitters with both selenophene and selenide groups can be seen.

Obviously, the EL efficiencies noticeably increase with the introduction of more -F substituents to the selenide group in the concerned phosphorescent emitter (Table 6). This result can be explained by both the energy-level layout in the emission layer of the OLEDs and the electronic features of these asymmetric heteroleptic Ir(III) phosphorescent emitters (Table 5, Figure 5, and Figures S18 and S23). Owing to the hole-injection capacity provided by the selenophene unit, the HOMO levels (ca. 5.20 eV) of these phosphorescent emitters are much higher than those of CBP (ca. 5.90 eV, Figure 5). Therefore, the holes injected into the emission layer of the OLEDs can be easily trapped by these phosphorescent emitters. On the other hand, their LUMO levels are very close to that of the host material CBP (ca. 2.50 eV, Figure 5). In addition, the CV results have shown that the fluorinated selenide groups can enhance the electron-injection capacity of these phosphorescent emitters. All of these results indicate that these phosphorescent emitters can be electronically excited by direct charge trapping.^{55–57} In view of their aforementioned high hole-trapping ability, the EL efficiencies of these asymmetric heteroleptic Ir(III) phosphorescent emitters should be mainly up to their electron-trapping capacity. From Ir-Se0F to Ir-Se3F, their LUMO levels decline gradually (Figure 5), indicating their gradually enhanced electron-trapping ability. The results of single-carrier devices demonstrate that the asymmetric heteroleptic Ir(III) complexes can show improved transporting ability for both holes and electrons. In addition, with an increase in the number of -F substituents on the selenide groups, their hole-transporting ability is reduced, while the electron-transporting ability is enhanced, indicating more balanced charge-transporting properties. Hence, Ir-Se3F shows the highest EL efficiencies among these complexes (Figure S23). The EL ability of these

Table 6. EL Performance of the Electrophosphorescent OLEDs

device	dopant (amt (wt %))	$V_{\text{turn-on}}$ (V)	luminance L_{max} (cd m^{-2}) ^a	η_{ext} (%)	η_{L} (cd A^{-1})	η_{p} (lm W^{-1})	λ_{max} (nm) ^d
A1	Ir-Se0F (6.0)	4.3	10730 (19.1)	13.3 (4.3) ^a	42.6 (4.3)	30.8 (4.3)	584 (0.59, 0.40)
				12.2 ^b	39.2	17.7	
				10.5 ^c	33.5	11.2	
A2	Ir-Se0F (8.0)	4.2	9119 (18.9)	15.2 (4.2)	49.4 (4.2)	37.0 (4.2)	584 (0.59, 0.41)
				11.9	38.5	16.6	
				8.9	28.8	9.2	
A3	Ir-Se0F (10.0)	4.2	10708 (18.4)	14.0 (4.2)	44.8 (4.2)	33.6 (4.2)	584 (0.59, 0.40)
				12.4	39.8	16.6	
				10.2	32.7	9.4	
B1	Ir-Se1F (6.0)	4.2	12053 (16.5)	13.9 (4.2)	40.1 (4.2)	30.0 (4.2)	584 (0.57, 0.41)
				13.2	38.0	19.8	
				11.9	34.4	13.7	
B2	Ir-Se1F (8.0)	3.8	8437 (20.3)	15.8 (3.8)	50.9 (3.8)	42.5 (3.8)	584 (0.59, 0.41)
				9.9	31.9	10.8	
				6.2	20.1	4.8	
B3	Ir-Se1F (10.0)	3.7	9950 (18.6)	8.2 (3.7)	26.6 (3.7)	22.8 (3.7)	584 (0.59, 0.41)
				5.7	18.5	7.8	
				3.7	12.1	3.6	
C1	Ir-Se2F (6.0)	4.8	12940 (14.4)	10.6 (4.8)	34.5 (4.8)	22.6 (4.8)	584 (0.59, 0.41)
				9.1	29.5	13.3	
				7.5	24.4	8.8	
C2	Ir-Se2F (8.0)	4.1	12628 (16.8)	18.2 (4.1)	58.4 (4.1)	44.5 (4.1)	584 (0.59, 0.41)
				16.5	53.0	26.2	
				14.4	46.4	17.8	
C3	Ir-Se2F (10.0)	4.1	12887 (16.8)	12.7 (4.1)	40.9 (4.1)	31.2 (4.1)	584 (0.59, 0.41)
				11.5	37.1	18.6	
				10.1	32.6	12.9	
D1	Ir-Se3F (6.0)	3.5	11817 (16.0)	18.5 (3.5)	60.0 (3.5)	54.3 (3.5)	584 (0.59, 0.41)
				17.0	55.2	31.3	
				14.8	48.1	20.5	
D2	Ir-Se3F (8.0)	3.6	10981 (16.9)	19.9 (3.2)	65.6 (3.6)	57.3 (3.6)	584 (0.58, 0.41)
				17.5	57.7	30.6	
				14.7	48.6	19.3	
D3	Ir-Se3F (10.0)	3.6	11410 (15.0)	15.7 (3.6)	51.9 (3.6)	45.1 (3.6)	584 (0.59, 0.41)
				14.4	47.7	27.1	
				13.1	43.3	19.8	

^aMaximum values of the devices. Values in parentheses are the voltages at which they were obtained (in V). ^bValues were collected at 100 cd m^{-2} . ^cValues were collected at 1000 cd m^{-2} . ^dValues were collected at 10 V, and CIE coordinates (x, y) are shown in parentheses.

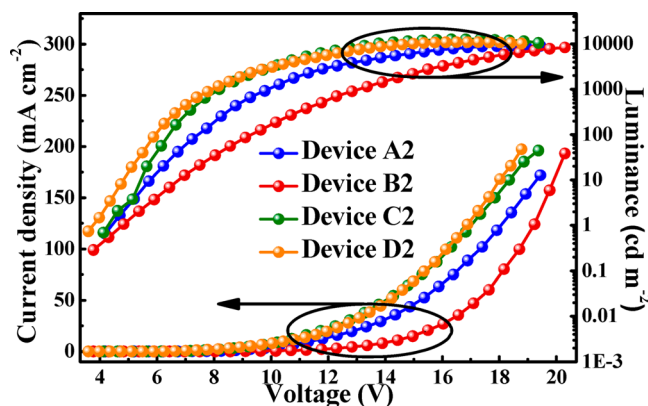


Figure 7. Current density–voltage–luminance (J – V – L) curves for optimized OLEDs.

asymmetric heteroleptic Ir(III) phosphorescent emitters falls in the order Ir-Se3F > Ir-Se2F > Ir-Se1F > Ir-Se0F (Table 6).

CONCLUSION

In conclusion, a series of asymmetric heteroleptic Ir(III) phosphorescent complexes have been successfully prepared through employing ppy-type ligands with selenophene and selenide groups. All of these novel asymmetric heteroleptic Ir(III) phosphorescent species can show high Φ_{p} values of ca. 0.90 to benefit their EL performances. It has also been found that the nature of their phosphorescent emission is mainly determined by the ppy-type ligand with a selenophene group, dominantly showing $^3\pi-\pi^*$ features. By an increase in the number of –F substituents on the selenide groups, the EL efficiencies of these asymmetric heteroleptic Ir(III) phosphorescent complexes can be obviously improved due to their enhanced electron-trapping behavior, which can balance their high hole-trapping ability. As a result, the optimized solution-processed OLED can show impressive EL efficiencies with a maximum η_{ext} value of 19.9%, η_{L} value of 65.6 cd A^{-1} , and η_{p} value of 57.3 lm W^{-1} , representing state of the art EL performance achieved by selenium-containing phosphorescent emitters. This research should clearly reveal the great potential

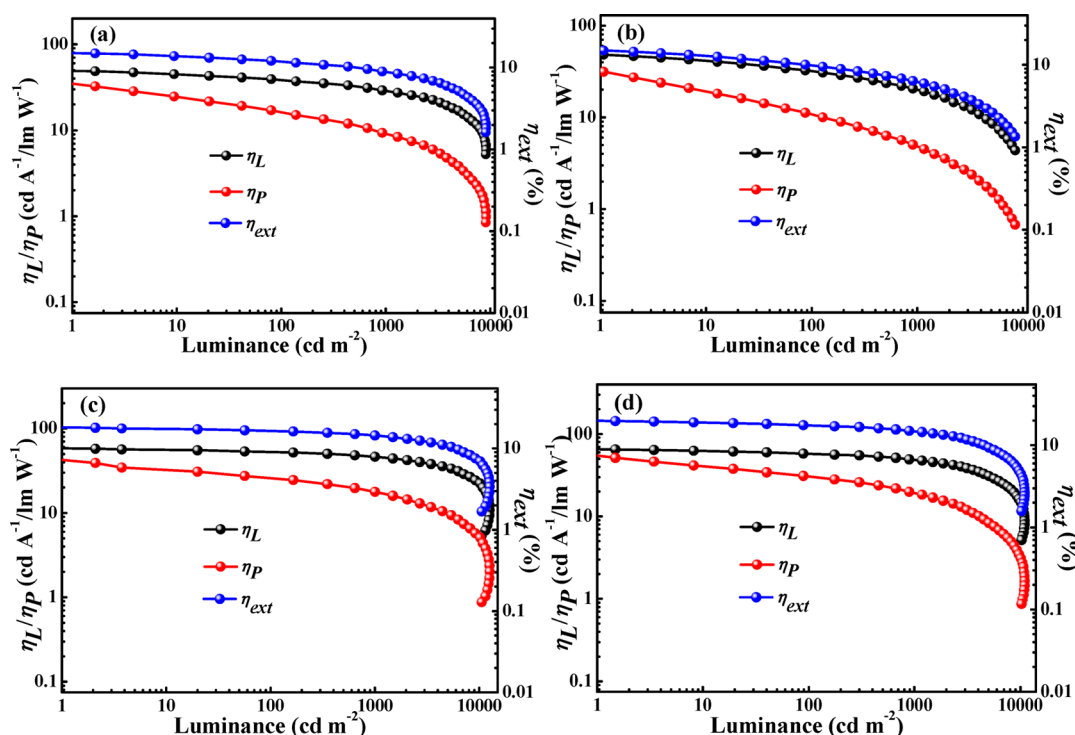


Figure 8. Relationship between EL efficiencies and luminance for the optimized devices: (a) device A2; (b) device B2; (c) device C2; (d) device D2.

selenium-containing groups have in the development of high-performance ppy-type Ir(III) phosphorescent emitters.

■ ASSOCIATED CONTENT

Supporting Information

The Supporting Information is available free of charge on the ACS Publications website at DOI: 10.1021/acs.inorgchem.8b01639.

Synthetic scheme via selenide intermediates, experimental scheme of the selenone group ($-\text{SeO}_2\text{Ar}$) reduction, structural data from X-ray crystallographic results for Ir-Se2F and Ir-Se3F, NMR spectra of all the obtained Ir(III) complexes and ligands, experimental HRMS and calculated isotopic distribution spectra of all the final Ir(III) complexes, electrochemical, thermal, and photophysical properties and IR data for all the final Ir(III) complexes, OLED fabrication and measurements, EL results for the devices except the optimized ones, and single-carrier devices with 8 wt % doped CBP films using the asymmetric heteroleptic Ir(III) complexes and $\text{Ir}(\text{ppy})_2(\text{acac})$ as active layer (PDF)

Accession Codes

CCDC 1819886–1819887 contain the supplementary crystallographic data for this paper. These data can be obtained free of charge via www.ccdc.cam.ac.uk/data_request/cif, or by emailing data_request@ccdc.cam.ac.uk, or by contacting The Cambridge Crystallographic Data Centre, 12 Union Road, Cambridge CB2 1EZ, UK; fax: +44 1223 336033.

■ AUTHOR INFORMATION

Corresponding Authors

*G.Z.: fax, +86-029-82663914; e-mail, zhougj@mail.xjtu.edu.cn.

*M.M.: e-mail, mmfyangling@126.com.

*Z.W.: e-mail, zhaoxinwu@mail.xjtu.edu.cn.

ORCID

Guijiang Zhou: 0000-0002-5863-3551

Zhaoxin Wu: 0000-0003-2979-3051

Notes

The authors declare no competing financial interest.

■ ACKNOWLEDGMENTS

This research was financially supported by the National Natural Science Foundation of China (21572176, 21602170), Fundamental Research Funds for the Central Universities (cxtd2015003 and 01091191320074), the China Postdoctoral Science Foundation (2015M580831 and 20130201110034), the Natural Science Foundation of Shaanxi Province (2016JM3035), and the Key Creative Scientific Research Team in Yulin City (2015cxy-25). Financial support from the State Key Laboratory for Mechanical Behavior of Materials is also acknowledged. We thank Miss Axin Lu at the Instrument Analysis Center of Xi'an Jiaotong University for her assistance with the analysis of HRMS data and simulation of spectral patterns (isotopic distribution) for all the obtained Ir(III) complexes.

■ REFERENCES

- (1) Fan, C.; Li, Y.; Yang, C.; Wu, H.; Qin, J.; Cao, Y. Phosphoryl/Sulfonyl-Substituted Iridium Complexes as Blue Phosphorescent Emitters for Single-Layer Blue and White Organic Light-Emitting Diodes by Solution Process. *Chem. Mater.* **2012**, *24*, 4581–4587.
- (2) Cho, W.; Sarada, G.; Lee, H.; Song, M.; Gal, Y.-S.; Lee, Y.; Jin, S.-H. Highly Efficient, Conventional and Flexible Deep-Red Phosphorescent OLEDs Using Ambipolar Thiophene/Selenophene-Phenylquinoline Ligand-Based Ir(III) Complexes. *Dyes Pigm.* **2017**, *136*, 390–397.
- (3) Liu, D.; Ren, H.; Deng, L.; Zhang, T. Synthesis and Electrophosphorescence of Iridium Complexes Containing Benzo-

thiazole-Based Ligands. *ACS Appl. Mater. Interfaces* **2013**, *5*, 4937–4944.

(4) Tan, G.; Chen, S.; Sun, N.; Li, Y.; Fortin, D.; Wong, W.-Y.; Kwok, H.-S.; Ma, D.; Wu, H.; Wang, L.; Harvey, P. D. Highly Efficient Iridium(III) Phosphors with Phenoxy-Substituted Ligands and Their High-Performance OLEDs. *J. Mater. Chem. C* **2013**, *1*, 808–821.

(5) Ho, C.-L.; Lam, C.-S.; Sun, N.; Ma, D.; Liu, L.; Yu, Z.-Q.; Xue, L.; Lin, Z.; Li, H.; Lo, Y. H.; Wong, W.-Y. Synthesis, Characterization and Electroluminescent Properties of Iridium(III) 2-Phenylpyridine-Type Complexes Containing Trifluoromethyl Substituents and Various Main-Group Moieties. *Isr. J. Chem.* **2014**, *54*, 999–1014.

(6) Mróz, W.; Ragni, R.; Galeotti, F.; Mesto, E.; Botta, C.; Cola, L. D.; Farinola, G. M.; Giovannella, U. Influence of Electronic and Steric Effects of Substituted Ligands Coordinated to Ir(III) Complexes on the Solution Processed OLED Properties. *J. Mater. Chem. C* **2015**, *3*, 7506–7512.

(7) Zhou, G.; Ho, C.-L.; Wong, W.-Y.; Wang, Q.; Ma, D.; Wang, L.; Lin, Z.; Marder, T. B.; Beeby, A. Manipulating Charge-Transfer Character with Electron-Withdrawing Main-Group Moieties for the Color Tuning of Iridium Electrophosphors. *Adv. Funct. Mater.* **2008**, *18*, 499–511.

(8) Benjamin, H.; Zheng, Y.; Batsanov, A. S.; Fox, M. A.; Al-Attar, H. A.; Monkman, A. P.; Bryce, M. R. Sulfonyl-Substituted Heteroleptic Cyclometalated Iridium(III) Complexes as Blue Emitters for Solution-Processable Phosphorescent Organic Light-Emitting Diodes. *Inorg. Chem.* **2016**, *55*, 8612–8627.

(9) Tan, G.; Chen, S.; Siu, C.-H.; Langlois, A.; Qiu, Y.; Fan, H.; Ho, C.-L.; Harvey, P. D.; Lo, Y. H.; Liu, L.; Wong, W.-Y. Platinum(II) Cyclometallates Featuring Broad Emission Bands and Their Applications in Color-Tunable OLEDs and High Color-Rendering WOLEDs. *J. Mater. Chem. C* **2016**, *4*, 6016–6026.

(10) Tsuboyama, A.; Iwawaki, H.; Furugori, M.; Mukaide, T.; Kamatani, J.; Igawa, S.; Moriyama, T.; Miura, S.; Takiguchi, T.; Okada, S. Homoleptic Cyclometalated Iridium Complexes with Highly Efficient Red Phosphorescence and Application to Organic Light-Emitting Diode. *J. Am. Chem. Soc.* **2003**, *125*, 12971–12979.

(11) Hudson, Z. M.; Sun, C.; Helander, M. G.; Amarné, H.; Lu, Z.-H.; Wang, S. Enhancing Phosphorescence and Electrophosphorescence Efficiency of Cyclometalated Pt(II) Compounds with Triarylboron. *Adv. Funct. Mater.* **2010**, *20*, 3426–3439.

(12) Sree, V. G.; Cho, W.; Shin, S.; Lee, T.; Gal, Y.-S.; Song, M.; Jin, S.-H. Highly Efficient Solution-Processed Deep-Red Emitting Heteroleptic Thiophene-Phenylquinoline Based Ir(III) Complexes for Phosphorescent Organic Light-Emitting Diodes. *Dyes Pigm.* **2017**, *139*, 779–787.

(13) Cho, Y. J.; Hong, S. A.; Son, H. J.; Han, W. S.; Cho, D. W.; Kang, S. O. Efficient Light Harvesting and Energy Transfer in a Red Phosphorescent Iridium Dendrimer. *Inorg. Chem.* **2014**, *53*, 13136–13141.

(14) Ikawa, S.; Yagi, S.; Maeda, T.; Nakazumi, H.; Fujiwara, H.; Koseki, S.; Sakurai, Y. Photo- and Electroluminescence from Deep-Red- and Near-Infrared-Phosphorescent Tris-Cyclometalated Iridium(III) Complexes Bearing Largely π -Extended Ligands. *Inorg. Chem. Commun.* **2013**, *38*, 14–19.

(15) Tsumimoto, H.; Yagi, S.; Honda, Y.; Terao, H.; Maeda, T.; Nakazumi, H.; Sakurai, Y. Photoluminescent Properties of Heteroleptic Cyclometalated Platinum(II) Complexes Bearing 1,3-Bis(3,4-Dibutoxyphenyl)propane-1,3-dionate as an Ancillary Ligand. *J. Lumin.* **2010**, *130*, 217–221.

(16) Yang, C.; Lai, S. L.; Chan, S. L.; Low, K. H.; Cheng, G.; Yeung, K. T.; Kwok, C. C.; Che, C. M. Phosphorescent Cyclometalated Iridium(III) Complexes That Contain Substituted 2-Acetylbenzo[b]-thiophen-3-olate Ligand for Red Organic Light-Emitting Devices. *Chem. - Asian J.* **2014**, *9*, 3572–3585.

(17) Sivchik, V. V.; Solomatina, A. I.; Chen, Y. T.; Karttunen, A. J.; Tunik, S. P.; Chou, P. T.; Koshevoy, I. O. Halogen Bonding to Amplify Luminescence: A Case Study Using a Platinum Cyclometalated Complex. *Angew. Chem., Int. Ed.* **2015**, *54*, 14057–14060.

(18) Bandini, M.; Bianchi, M.; Valenti, G.; Piccinelli, F.; Paolucci, F.; Monari, M.; Umami-Ronchi, A.; Marcaccio, M. Electrochemiluminescent Functionalizable Cyclometalated Thiophene-Based Iridium(III) Complexes. *Inorg. Chem.* **2010**, *49*, 1439–1448.

(19) Li, T. Y.; Liang, X.; Zhou, L.; Wu, C.; Zhang, S.; Liu, X.; Lu, G. Z.; Xue, L. S.; Zheng, Y. X.; Zuo, J. L. *N*-Heterocyclic Carbenes: Versatile Second Cyclometalated Ligands for Neutral Iridium(III) Heteroleptic Complexes. *Inorg. Chem.* **2015**, *54*, 161–173.

(20) Shigehiro, T.; Chen, Q.; Yagi, S.; Maeda, T.; Nakazumi, H.; Sakurai, Y. Substituent Effect on Photo- and Electroluminescence Properties of Heteroleptic Cyclometalated Platinum(II) Complexes Based on a 2-(Dibenzo[b,d]furan-4-yl)pyridine Ligand. *Dyes Pigm.* **2016**, *124*, 165–173.

(21) Chau, N.-Y.; Ho, P.-Y.; Ho, C.-L.; Ma, D.; Wong, W.-Y. Color-Tunable Thiazole-Based Iridium(III) Complexes: Synthesis, Characterization and Their OLED Applications. *J. Organomet. Chem.* **2017**, *829*, 92–100.

(22) Giridhar, T.; Cho, W.; Park, J.; Park, J.-S.; Gal, Y.-S.; Kang, S.; Lee, J. Y.; Jin, S.-H. Facile Synthesis and Characterization of Iridium(III) Complexes Containing an *N*-Ethylcarbazole–Thiazole Main Ligand Using a Tandem Reaction for Solution Processed Phosphorescent Organic Light-Emitting Diodes. *J. Mater. Chem. C* **2013**, *1*, 2368–2378.

(23) Feng, Y.; Li, P.; Zhuang, X.; Ye, K.; Peng, T.; Liu, Y.; Wang, Y. A Novel Bipolar Phosphorescent Host for Highly Efficient Deep-Red OLEDs at a Wide Luminance Range of 1000–10 000 cd m⁻². *Chem. Commun.* **2015**, *51*, 12544–12547.

(24) Wang, R.; Liu, D.; Ren, H.; Zhang, T.; Wang, X.; Li, J. Homoleptic Tris-Cyclometalated Iridium Complexes with 2-Phenylbenzothiazole Ligands for Highly Efficient Orange OLEDs. *J. Mater. Chem.* **2011**, *21*, 15494–15500.

(25) Tavasli, M.; Bettington, S.; Perepichka, I. F.; Batsanov, A. S.; Bryce, M. R.; Rothe, C.; Monkman, A. P. A Tris-Cyclometalated Iridium(III) Complex of 2-(5,5-Dioxido-dibenzothiophen-3-yl)pyridine: Synthesis, Structural, Redox and Photophysical Properties. *Eur. J. Inorg. Chem.* **2007**, *2007*, 4808–4814.

(26) Fernandes, A. P.; Gandin, V. Selenium Compounds as Therapeutic Agents in Cancer. *Biochim. Biophys. Acta, Gen. Subj.* **2015**, *1850*, 1642–1660.

(27) Al-Hashimi, M.; Han, Y.; Smith, J.; Bazzi, H. S.; Alqaradawi, S. Y. A.; Watkins, S. E.; Anthopoulos, T. D.; Heeney, M. Influence of the Heteroatom on the Optoelectronic Properties and Transistor Performance of Soluble Thiophene-, Selenophene- and Tellurophene–Vinylene Copolymers. *Chem. Sci.* **2016**, *7*, 1093–1099.

(28) Ashraf, R. S.; Meager, I.; Nikolka, M.; Kirkus, M.; Planells, M.; Schroeder, B. C.; Holliday, S.; Hurhangee, M.; Nielsen, C. B.; Siringhaus, H.; McCulloch, I. Chalcogenophene Comonomer Comparison in Small Band Gap Diketopyrrolopyrrole-Based Conjugated Polymers for High-Performing Field-Effect Transistors and Organic Solar Cells. *J. Am. Chem. Soc.* **2015**, *137*, 1314–1321.

(29) Gao, D.; Gibson, G. L.; Hollinger, J.; Li, P.; Seferos, D. S. 'Blocky' Donor–Acceptor Polymers Containing Selenophene, Benzothienophene and Thienothiophene for Improved Molecular Ordering. *Polym. Chem.* **2015**, *6*, 3353–3360.

(30) Xu, X.; Yang, X.; Dang, J.; Zhou, G.; Wu, Y.; Li, H.; Wong, W. Y. Trifunctional Ir(III) Ppy-Type Asymmetric Phosphorescent Emitters with Ambipolar Features for Highly Efficient Electroluminescent Devices. *Chem. Commun.* **2014**, *50*, 2473–2476.

(31) Xu, X.; Yang, X.; Wu, Y.; Zhou, G.; Wu, C.; Wong, W. Y. Tris-Heteroleptic Cyclometalated Iridium(III) Complexes with Ambipolar or Electron Injection/Transport Features for Highly Efficient Electrophosphorescent Devices. *Chem. - Asian J.* **2015**, *10*, 252–262.

(32) Xu, X.; Guo, H.; Zhao, J.; Liu, B.; Yang, X.; Zhou, G.; Wu, Z. Asymmetric Tris-Heteroleptic Iridium^{III} Complexes Containing a 9-Phenyl-9-phosphaphluorene Oxide Moiety with Enhanced Charge Carrier Injection/Transporting Properties for Highly Efficient Solution-Processed Organic Light-Emitting Diodes. *Chem. Mater.* **2016**, *28*, 8556–8569.

- (33) Hofbeck, T.; Yersin, H. The Triplet State of *fac*-Ir(ppy)₃. *Inorg. Chem.* **2010**, *49*, 9290–9299.
- (34) Sheldrick, G. M. *SHELXL-97, Program for Crystal Structure Refinement*; University of Göttingen: Göttingen, Germany, 1997.
- (35) Sheldrick, G. M. *SADABS*; University of Göttingen: Göttingen, Germany, 1996.
- (36) Wadt, W. R.; Hay, P. J. Ab Initio Effective Core Potentials for Molecular Calculations. Potentials for Main Group elements Na to Bi. *J. Chem. Phys.* **1985**, *82*, 284–298.
- (37) Hay, P. J.; Wadt, W. R. Ab Initio Effective Core Potentials for Molecular Calculations. Potentials for K to Au Including the Outermost Core Orbitals. *J. Chem. Phys.* **1985**, *82*, 299–310.
- (38) Frisch, M. J.; Trucks, G. W.; Schlegel, H. B.; Scuseria, G. E.; Robb, M. A.; Cheeseman, J. R.; Scalmani, G.; Barone, V.; Mennucci, B.; Petersson, G. A.; Nakatsuji, H.; Caricato, M.; Li, X.; Hratchian, H. P.; Izmaylov, A. F.; Bloino, J.; Zheng, G.; Sonnenberg, J. L.; Hada, M.; Ehara, M.; Toyota, K.; Fukuda, R.; Hasegawa, J.; Ishida, M.; Nakajima, T.; Honda, Y.; Kitao, O.; Nakai, H.; Vreven, T.; Montgomery, J. A., Jr.; Peralta, J. E.; Ogliaro, F.; Bearpark, M.; Heyd, J. J.; Brothers, E.; Kudin, K. N.; Staroverov, V. N.; Kobayashi, R.; Normand, J.; Raghavachari, K.; Rendell, A.; Burant, J. C.; Iyengar, S. S.; Tomasi, J.; Cossi, M.; Rega, N.; Millam, J. M.; Klene, M.; Knox, J. E.; Cross, J. B.; Bakken, V.; Adamo, C.; Jaramillo, J.; Gomperts, R.; Stratmann, R. E.; Yazyev, O.; Austin, A. J.; Cammi, R.; Pomelli, C.; Ochterski, J. W.; Martin, R. L.; Morokuma, K.; Zakrzewski, V. G.; Voth, G. A.; Salvador, P.; Dannenberg, J. J.; Dapprich, S.; Daniels, A. D.; Farkas, O.; Foresman, J. B.; Ortiz, J. V.; Cioslowski, J.; Fox, D. J. *Gaussian 09, Revision A.01*; Gaussian, Inc.: Wallingford, CT, 2009.
- (39) Singh, D.; Deobald, A. M.; Camargo, L. R.; Tabarelli, G.; Rodrigues, O. E.; Braga, A. L. An Efficient One-Pot Synthesis of Symmetrical Diselenides or Ditellurides from Halides with CuO Nanopowder/Se⁰ or Te⁰/Base. *Org. Lett.* **2010**, *12*, 3288–3291.
- (40) Alves, D.; Santos, C. G.; Paixão, M. W.; Soares, L. C.; Souza, D. d.; Rodrigues, O. E. D.; Braga, A. L. CuO Nanoparticles: An Efficient and Recyclable Catalyst for Cross-Coupling Reactions of Organic Diselenides with Aryl Boronic Acids. *Tetrahedron Lett.* **2009**, *50*, 6635–6638.
- (41) Bhadra, S.; Saha, A.; Ranu, B. C. Al₂O₃-Supported Cu-Catalyzed Electrophilic Substitution by PhSeBr in Organoboranes, Organosilanes, and Organostannanes. A Protocol for the Synthesis of Unsymmetrical Diaryl and Alkyl Aryl Selenides. *J. Org. Chem.* **2010**, *75*, 4864–4867.
- (42) Stille, J. K.; Lau, K. S. Y. Mechanisms of Oxidative Addition of Organic Halides to Group 8 Transition-Metal Complexes. *Acc. Chem. Res.* **1977**, *10*, 434–442.
- (43) Jutand, A.; Mosleh, A. Rate and Mechanism of Oxidative Addition of Aryl Triflates to Zerovalent Palladium Complexes. Evidence for the Formation of Cationic (σ -Aryl)palladium Complexes. *Organometallics* **1995**, *14*, 1810–1817.
- (44) Espinet, P.; Echavarren, A. M. The Mechanisms of the Stille Reaction. *Angew. Chem., Int. Ed.* **2004**, *43*, 4704–4734.
- (45) Tamura, Y.; Hisamatsu, Y.; Kazama, A.; Yoza, K.; Sato, K.; Kuroda, R.; Aoki, S. Stereospecific Synthesis of Tris-heteroleptic Tris-cyclometalated Iridium(III) Complexes via Different Heteroleptic Halogen-Bridged Iridium(III) Dimers and Their Photophysical Properties. *Inorg. Chem.* **2018**, *57*, 4571–4589.
- (46) Sprouse, S.; King, K. A.; Spellane, P. J.; Watts, R. J. Photophysical Effects of Metal-Carbon σ Bonds in Ortho-Metalated Complexes of Ir(III) and Rh(III). *J. Am. Chem. Soc.* **1984**, *106*, 6647–6653.
- (47) Li, G.; Xu, L.; Zhang, W.; Zhou, K.; Ding, Y.; Liu, F.; He, X.; He, G. Narrow-Bandgap Chalcogenoviologens for Electrochromism and Visible-Light-Driven Hydrogen Evolution. *Angew. Chem.* **2018**, *130*, 4991–4995.
- (48) Lamansky, S.; Djurovich, P.; Murphy, D.; Abdel-Razzaq, F.; Lee, H. E.; Adachi, C.; Burrows, P. E.; Forrest, S. R.; Thompson, M. E. Highly Phosphorescent Bis-Cyclometalated Iridium Complexes: Synthesis, Photophysical Characterization, and Use in Organic Light Emitting Diodes. *J. Am. Chem. Soc.* **2001**, *123*, 4304–4312.
- (49) Spellane, P.; Watts, R. J.; Vogler, A. Luminescence Characterizations of Cyclometalated Rhenium(I) Carbonyl Complexes. *Inorg. Chem.* **1993**, *32*, 5633–5636.
- (50) Wasserberg, D.; Meskers, S. C.; Janssen, R. A. Phosphorescent Resonant Energy Transfer between Iridium Complexes. *J. Phys. Chem. A* **2007**, *111*, 1381–1388.
- (51) Cho, Y. J.; Kim, S. Y.; Son, H. J.; Han, W. S.; Cho, D. W.; Kang, S. O. Comprehensive Spectroscopic Studies of *Cis* and *Trans* Isomers of Red-Phosphorescent Heteroleptic Iridium(III) Complexes. *J. Photochem. Photobiol., A* **2018**, *356*, 673–680.
- (52) Yoshihara, T.; Hosaka, M.; Terata, M.; Ichikawa, K.; Murayama, S.; Tanaka, A.; Mori, M.; Itabashi, H.; Takeuchi, T.; Tobita, S. Intracellular and in Vivo Oxygen Sensing Using Phosphorescent Ir(III) Complexes with a Modified Acetylacetonato Ligand. *Anal. Chem.* **2015**, *87*, 2710–2717.
- (53) Tsutsui, T. Progress in Electroluminescent Devices Using Molecular Thin Films. *MRS Bull.* **1997**, *22*, 39–45.
- (54) Mao, H.; Zang, C.; Wen, L.; Shan, G.; Sun, H.; Xie, W.; Su, Z. Ir(III) Phosphors Modified with Fluorine Atoms in Pyridine-1,2,4-triazolyl Ligands for Efficient OLEDs Possessing Low-Efficiency Roll-off. *Organometallics* **2016**, *35*, 3870–3877.
- (55) Zhang, X.; Gao, J.; Yang, C.; Zhu, L.; Li, Z.; Zhang, K.; Qin, J.; You, H.; Ma, D. Highly Efficient Iridium(III) Complexes with Diphenylquinoline Ligands for Organic Light-Emitting Diodes: Synthesis and Effect of Fluorinated Substitutes on Electrochemistry, Photophysics and Electroluminescence. *J. Organomet. Chem.* **2006**, *691*, 4312–4319.
- (56) Rhee, S. H.; Kim, S. H.; Kim, H. S.; Shin, J. Y.; Bastola, J.; Ryu, S. Y. Heavily Doped, Charge-Balanced Fluorescent Organic Light-Emitting Diodes from Direct Charge Trapping of Dopants in Emission Layer. *ACS Appl. Mater. Interfaces* **2015**, *7*, 16750–16759.
- (57) Tao, Y.; Yang, C.; Qin, J. Organic Host Materials for Phosphorescent Organic Light-Emitting Diodes. *Chem. Soc. Rev.* **2011**, *40*, 2943–2970.